HHS Public Access

Author manuscript

Nat Genet. Author manuscript; available in PMC 2022 October 01.

Published in final edited form as:

Nat Genet. 2021 December ; 53(12): 1649–1663. doi:10.1038/s41588-021-00946-4.

Renal plasticity revealed through reversal of polycystic kidney disease in mice

Ke Dong[1], **Chao Zhang**[1], **Xin Tian**[1], **Daniel Coman**[2], **Fahmeed Hyder**[2,3], **Ming Ma**[1], **Stefan Somlo**[1,4,‡]

[1]Department of Internal Medicine, Yale School of Medicine, New Haven, Connecticut, USA

[2]Department of Radiology and Biomedical Imaging, Yale School of Medicine, New Haven, Connecticut, USA

[3]Department of Biomedical Engineering, Yale School of Medicine, New Haven, Connecticut, USA

[4]Department of Genetics, Yale School of Medicine, New Haven, Connecticut, USA.

Abstract

Initiation of cyst formation in autosomal dominant polycystic kidney disease (ADPKD) occurs when kidney tubule cells are rendered null for either *PKD1* or *PKD2* by somatic "second hit" mutations. Subsequent cyst progression remodels the organ through changes in tubule cell shape, proliferation and secretion. The kidney develops inflammation and fibrosis. We constructed a mouse model in which adult inactivation of either Pkd gene can be followed by reactivation of the gene at a later time. Using this model, we show that re-expression of Pkd genes in cystic kidneys results in rapid reversal of ADPKD. Cyst cell proliferation is reduced, autophagy is activated, and cystic tubules with expanded lumens lined by squamoid cells revert to normal lumens lined by cuboidal cells. Increases in inflammation, extracellular matrix deposition and myofibroblast activation are reversed, and the kidneys become smaller. We conclude that phenotypic features of ADPKD are reversible and that the kidney has an unexpected capacity for plasticity controlled at least in part by ADPKD gene function.

Autosomal dominant polycystic kidney disease (ADPKD) is a common genetic disease caused primarily by mutations in *PKD1* and *PKD2*, which encode polycsytin-1 (PC1) and polycystin-2 (PC2), respectively[1]. Clinical hallmarks of ADPKD include growth of fluid-filled cysts that deform and enlarge the kidneys and set off secondary processes such as inflammation and fibrosis that result in renal failure in a majority of patients. Somatic "second hit" somatic mutations affecting the normal allele of either gene in kidney tubule cells are sufficient to initiate cysts[2,3], following which additional factors modulate cyst progression[4]. These factors include the developmental timing of Pkd gene inactivation[5–7],

‡ stefan.somlo@yale.edu .

Author Contributions

K.D., C.Z., X.T., and M.M. performed experiments. D.C. and F.H. performed and analyzed the MRI studies. S.S. conceived the study, and K.D. and S.S. designed the study and analyzed data. K.D. and S.S. prepared the figures, and S.S. wrote the manuscript with input from all the authors.

Competing Interests

The authors declare no competing interests.

the occurrence of acute kidney injury[8–11] and the nature of the inflammatory response[12–16]. Functional dosage variation of PC1, either due to the type of mutation in *PKD1*[17] or due altered biogenesis of PC1[18,19], further modify disease severity. Mouse models based on the orthologous genes *Pkd1* or *Pkd2* have contributed to understanding the in vivo mechanisms of ADPKD and have been used for preclinical evaluation of therapies[20–23]. Biological processes altered in cystic epithelia include cyclic AMP-dependent signaling[24,25], G-protein signaling[26–28], mammalian target of rapamycin (mTOR)[29–31], calcium signaling[32–34], growth factor receptor function[28,35], cell cycle regulation[36], cell matrix interactions[37,38], the epigenome[39], functioning of mitochondria[40–44] and Wnt signaling[45]. Cyst growth requires proliferation and transepithelial secretion by cyst epithelial cells[24,46,47]. The primary cilium, a solitary microtubule-based structure projecting into the lumen from the apical surface of tubule cells, has a central role in the pathogenesis of ADPKD[48,49], but the molecular functions of polycystins in cilia remain incompletely defined[46].

While slowing cyst progression is a valuable preclinical approach, we sought to determine whether ADPKD can be reversed by functional re-expression of the causative Pkd gene at physiological levels in vivo. We developed a mouse model for inactivation and subsequent reactivation of *Pkd2* and *Pkd1* to address this question. We used doxycycline inducible Cre–*lox*P for Pkd gene inactivation followed by tamoxifen inducible Flp–*FRT* for gene reactivation. We found that cyst formation is reversible. Dilated cystic structures lined by flattened epithelial cells revert to normal appearing nephrons with columnar epithelium. These changes are accompanied by a decrease in total kidney volume and by molecular changes showing increased autophagic flux and decreases in tubule cell proliferation, kidney inflammation, extracellular matrix deposition, and myofibroblast activation. In early stage cystic kidneys, these changes occur within 1 week of re-expression of polycystin. Re-expression at more advanced stages of ADPKD results in significant but less complete reversal of structural and molecular changes. Together, these studies show the unexpected capacity of the kidney to repair substantial structural changes under the control of polycystins.

Results

Re-activation allele for *Pkd2*.

We established a mouse model system for inducible kidney-selective inactivation of *Pkd2* followed by inducible reactivation at a later time point. Initial inactivation of *Pkd2* along the kidney tubule utilized the doxycycline inducible $Pax8^{rtTA}; TetO^{Cre}$ digenic system[46]. The subsequent reactivation step was controlled with by tamoxifen inducible optimized FLPe recombinase, FlpoER, expressed from the ROSA26 locus ($Rosa26^{FlpoER}$)[50] (Supplementary Note and Supplementary Fig. 1). The target allele for *Pkd2* reactivation was produced by modification of a bacterial artificial chromosome (BAC) with insertion of a transcriptional stop sequence flanked by *FRT* sites[51] into the first intron of *Pkd2* and of a triple-HA epitope tag sequence immediately before the termination codon (Supplementary Note and Supplementary Fig. 2). This modified $Pkd2^{FSF}$ BAC was used to generate transgenic mouse lines for in vivo re-expression (Supplementary Note). When combined with $Rosa26^{FlpoER}$ in the absence tamoxifen induction, these mice do not express the PC2-HA protein encoded

by *Pkd2*^{FSF} (Fig. 1a). Following 7 daily doses of tamoxifen beginning at age 13 weeks, PC2-HA is expressed in multiple tissues in 16-week-old mice (Fig. 1a). The onset of expression is rapid, with PC2-HA detectable in the kidney one week after starting tamoxifen (Fig. 1b). Once activated, PC2-HA is expressed throughout the kidney (Fig. 1c,d). The expression of PC2-HA from the *Pkd2*^{FSF}-BAC is transgene is ~1.5-fold compared to endogenous PC2 expression (Supplementary Fig. 3). PC2-HA expression from the combination of *Pkd2*^{FSF} with *Rosa26*^{FlpoER} is effectively silenced until induced with tamoxifen, after which there is rapid, broad, near physiological expression of PC2 in the kidney.

Re-activation of *Pkd2* reverses cyst formation.

We used this system to examine the effects of sequential *Pkd2* inactivation followed by reactivation on kidney structure and function. Experimental mice had the following six allele genotype: *Pkd2*$^{fl/-}$; *Pkd2*^{FSF}; *Pax8*^{rtTA}; *TetO*^{Cre}; *Rosa26*^{FlpoER}, abbreviated *Pkd2*$^{Cre/Flpo}$. "Non-cystic" control mice had the genotype *Pkd2*$^{fl/-}$; *Pkd2*^{FSF}; *TetO*^{Cre}; *Rosa26*^{FlpoER} lacking *Pax8*^{rtTA}. All alleles were heterozygous in experimental mice to control for potential phenotypic variation due to allele dosage. All mice received oral doxycycline for two weeks from postnatal day 28 to 42 (P28–42) to in inactivate *Pkd2*^{fl} in *Pkd2*$^{Cre/Flpo}$ mice and render much of the nephron null for PC2[46]. These mice showed significantly increased kidney weight to body weight ratio (KW/BW), percentage sagittal cross-sectional cystic area (cystic index, CI), and blood urea nitrogen (BUN) at 16 weeks age (Supplementary Note, Fig. 1e–h and Supplementary Fig. 4).

To determine the effects of PC2-HA re-expression, *Pkd2*$^{Cre/Flpo}$ mice were treated sequentially with doxycycline from P28–42 to inactivate *Pkd2*^{fl} followed by tamoxifen for 7 days beginning at 13 weeks age to induce re-expression of PC2-HA from the *Pkd2*^{FSF} transgene. Mice were examined at 13, 14 and 16 weeks of age (Fig. 1e–h and Supplementary Fig. 4). Thirteen-week-old mice, coincident with the time immediately before starting PC2-HA re-expression, had discernible polycystic kidney disease with cyst formation and kidney enlargement. When examined at 16 weeks of age, mice re-expressing PC2-HA beginning at 13 weeks had normal KW/BW ratio, CI and BUN, showing resolution of the changes that were present at 13 weeks (Fig. 1e–h and Supplementary Fig. 4). This effect was dependent on re-expression of PC2-HA (Supplementary Fig. 5). The decrease in kidney size and resolution of cysts was apparent at 14 weeks age, 7 days after starting re-expression of PC2-HA (Fig. 1e–h and Supplementary Fig. 4). Histological examination confirmed the presence of substantial cystic changes at 13 weeks with apparent resolution of these pre-existing changes at 14 and 16 weeks, i.e., 1 and 3 weeks, respectively, after the start PC2-HA re-expression (Fig. 1i). The pace of reversal of the polycystic phenotype is relatively rapid compared to the rate of cyst formation (Fig. 1j). These data show the remarkable and unexpected plasticity of the kidney tubule structure in response to loss and subsequent re-expression of PC2.

In vivo monitoring of ADPKD following PC2 re-expression.

The conclusion that re-expression of PC2-HA caused reversal of the polycystic disease in the above studies was inferred from comparison of mice undergoing different treatments and endpoints in parallel. We complemented these studies with longitudinal examination

of *Pkd2*$^{Cre/Flpo}$ mice using volumetric kidney magnetic resonance imaging (MRI) scans measured by an observer blinded to mouse genotype and treatment. *Pkd2*$^{Cre/Flpo}$ mice received either no treatment with doxycycline or tamoxifen ("non-cystic") or treatment only with doxycycline from P28–42 ("cystic") or treatment with doxycycline followed by tamoxifen for 7 days beginning at week 13 ("re-expression"). MRIs were performed at 13, 16 and 19 weeks age (Fig. 2a–c, Supplementary Table 1 and Supplementary Fig. 6a–c). Kidney volumes measured by MRI showed excellent correlation with kidney weight and KW/BW measured at week 19 (Supplementary Fig. 6d). Mice with inactivation of PC2 had progressive increase in kidney volume over the 6-week study while mice with inactivation of PC2 followed by re-expression of PC2-HA at 13 weeks showed progressive decrease in kidney volumes over 6 weeks (Fig. 2a–c, Supplementary Table 1 and Supplementary Fig. 6a–c).

The mean fold increase in kidney volume between 13 and 19 weeks in cystic mice was ~3.2-fold (Supplementary Table 1). The mean fold decrease in kidney volume in the re-expression group was ~3.2-fold. In keeping with the rapid response of kidney size to PC2-HA re-expression (Fig. 1j), most of the decrease in kidney volume was present at that first follow-up MRI at 16 weeks (Fig. 2b,c). Histological examination of the kidneys at 19 weeks showed marked cystic changes accompanied by proteinaceous casts in cyst lumens and inflammatory infiltrates in mice without PC2-HA re-expression (Fig. 2d). Three of four mice with PC2-HA re-expression showed generally normal histology without evidence of cysts, inflammation, or fibrosis (Fig. 2d). The kidney function at 19 weeks was normal following PC2-HA re-expression in the 3 mice with normal histology. One mouse in the MRI study had particularly large kidneys at week 13 (3,510 mm^3) and showed ~6.7-fold decrease in kidney volume to 521 mm^3 after PC2-HA was reactivated (Supplementary Table 1 and Supplementary Fig. 6c). This mouse had BUN 47 at 19 weeks, substantially better than mice without PC2 re-expression (Supplementary Table 1). Histological examination of this mouse showed areas of normal appearing tubules, but it had significant residual fibrosis and tubular atrophy, and some inflammatory infiltrates (Fig. 2e). The severity of polycystic disease at the time of intervention likely impacts the degree to which recovery can occur (see below). Nonetheless, these findings show that ADPKD is truly reversible at the whole organ level, including resolution of changes in total kidney volume.

Altered cellular programs after *Pkd2* reactivation in cysts.

Inactivation of polycystins leads to change from cuboidal tubule cell morphology to a flattened and spread-out epithelium[15,52–54]. Cells in all nephron segments show the flattened shape at 13 weeks age in *Pkd2*$^{Cre/Flpo}$ mice treated with doxycycline to inactivate *Pkd2* (Fig. 3a,b and Supplementary Fig. 7a–c). Re-expression of PC2-HA results in progressive reversion to cuboidal structure and reversal of lumen dilation along all nephron segments (Fig. 3c–h and Supplementary Fig. 7d–l). Cuboidal cell shape is already apparent 1 week after the start of PC2-HA reactivation, although the tubule lumens still show some residual dilation (Fig. 3c,d). By age 16 weeks, cells are cuboidal and luminal dilation appears resolved by re-expression of PC2-HA (Fig. 3e–h). In the absence of PC2-HA re-expression, the flattened cellular morphology and cysts persist (Fig. 3i–k and Supplementary Fig. 7m–

o). These findings show the occurrence of polycystin-dependent plasticity of the kidney that manifests through regulation of the structure of tubules and their component cells.

We considered whether apoptosis has a role in the rapid tissue remodeling following reactivation of PC2. While there was a mild transient apoptotic response at 14 weeks, this response did not persist and did not appear to be a major contributor the resolution of polycystic kidney phenotype (Supplementary Note and Supplementary Fig. 8). We next examined autophagy, a dynamic recycling mechanism active during cellular remodeling[55] that is essential for the maintenance of kidney homeostasis[56]. Mice were fasted for 20 hours to initiate autophagy and then treated with bafilomycin A_1 for 2 hours to block fusion between autophagosomes and lysosomes before harvesting kidney tissue. The autophagic flux under these conditions was measured by relative expression of LC3-II in kidney tissue lysates. *Pkd2* knockout kidneys showed significantly lower autophagic flux than non-cystic kidneys, indicating reduced autophagy in ADPKD in vivo (Fig. 3l,m). One week after re-expression of PC2, autophagic flux increased significantly to levels higher than observed in age matched non-cystic mice (Fig. 3l,m). Immunostaining with anti-LC3–II in kidney sections from the 14-week mice showed punctate cytoplasmic staining indicative of autophagosomes with a qualitative pattern relative to non-cystic controls that was reduced in cystic kidneys and increased in kidneys following re-expression of PC2 (Supplementary Fig. 9). Autophagy is reduced in mouse kidneys following loss of PC2, and this is reversed and further increased by re-expression of PC2, offering the hypothesis that the reparative remodeling of the kidney following polycystin re-expression occurs at least in part through enhanced autophagic flux.

Another hallmark of cyst growth following loss of polycystins is a low level but significant increase in cyst lining cell proliferation in all affected nephron segments[18,38,46,57–59]. We assessed cyst cell proliferation in $Pkd2^{Cre/Flpo}$ mice 1 and 3 weeks after initiation of PC2-HA re-expression using EdU incorporation and Ki67 staining (Fig. 4). Mice with and without PC2-HA re-expression at 13 weeks were injected with EdU 4 hours before euthanasia and the percentage of EdU or Ki67 positive nuclei were determined in cells of proximal tubule and collecting duct origin at 14 and 16 weeks. By either measure, ~4–6% of cells were proliferating in both segments at both time points in cystic kidneys without PC2-HA re-expression (Fig. 4a–d). Re-expression of PC2-HA resulted in a significant decrease in proliferation rates at both time points in both nephron segments (Fig. 4a–d). At 16 weeks, proliferation rates following re-expression were not significantly different from non-cystic control levels (Fig. 4c,d). This was also true at 14 weeks when analyzed by EdU incorporation, but Ki67 expression in the collecting duct showed persistence of a low level of elevated proliferation at this early time point (Fig. 4a,b). Overall, re-expression of PC2-HA results in the rapid and complete reversal of the increased proliferation in cyst lining cells in ADPKD.

Cyclin-D1 functions to support cellular proliferation and prevent quiescence[60]. In ADPKD, cyclin-D1 is upregulated in polycystin null cells[61] and in polycystic kidneys from adult mice[62]. We confirmed the changes in cyclin-D1 transcript expression in ADPKD models based on *Pkd1* and *Pkd2* (Supplementary Fig. 10a). $Pkd1^{fl/fl}; Pax8^{rtTA}; TetO^{Cre}$ mice induced with doxycycline from P28–42 had elevated levels cyclin-D1 at 10 weeks age when

there was only mild tubule dilation, indicating that elevated cyclin-D1 is an early finding in ADPKD models (Supplementary Fig. 10b). Concomitant inactivation of cilia, which markedly reduces cyst growth, also eliminated the rise in cyclin-D1, further confirming the correlation of cyclin-D1 levels with cyst-forming potential in vivo (Supplementary Fig. 10b). We found that cyclin-D1 protein levels show progressive elevation in kidney lysates from early (13 weeks) to late (16 weeks) stage polycystic disease in *Pkd2*$^{Cre/Flpo}$ mice without PC2-HA re-expression (Fig. 4e–h). Cyclin-D1 expression resolved to normal levels at 14 and 16 weeks age after re-expression of PC2-HA (Fig. 4e–h), showing that cyclin-D1 expression is correlated with cyst formation and cyst reversal, and suggesting a possible functional role for cyclin-D1 in cyst cell proliferation. The rapid normalization of tubule cell proliferation one week after initiation of re-expression of PC2 is one mechanistic element contributing to the reversal of ADPKD in mouse models.

Effects of PC2 re-expression on inflammatory changes.

Changes in cell shape, autophagy and proliferation specifically affect the cells along the nephron that comprise the cyst linings after loss of polycystin expression. Beyond direct effects on these cells, there are non-cell autonomous effects of cyst initiation and growth that affect the whole kidney and contribute to the progressive loss of kidney function[40]. Prominent among these are the increased presence of inflammatory mediators[16,63]. The chemokine Mcp-1 is elevated in cyst fluid and urine of ADPKD patients and decreases following treatment[64,65]. In mouse models, upregulation of Mcp-1 in the cyst cells promotes accumulation of circulating monocytes that contribute to ADPKD severity[15]. Mcp-1 mRNA levels are elevated at 16 weeks in cystic *Pkd2*$^{Cre/Flpo}$ mice, but are normal in kidneys with PC2 HA re-expression, supporting the correlation of whole kidney Mcp-1 levels with severity of polycystic disease (Supplementary Fig. 11a). ADPKD kidneys have an increased burden of macrophages, and experimental depletion of macrophages improves kidney function in ADPKD models[12,14], whereas increased expression of macrophages worsens disease severity[66,67]. In keeping with these studies, we observed progressive increase in F4/80 mRNA levels in *Pkd2* mutant kidneys at 13, 14 and 16 weeks (Fig. 5a,c) and this was associated with pericystic infiltrates of F4/80 positive cells (Fig. 5b,d). Re-expression of PC2-HA beginning at 13 weeks resulted in normalized levels of F4/80 mRNA at 14 and 16 weeks (Fig. 5a,c) and significantly reduced presence F4/80 positive cells in tissue sections (Fig. 5b,d). Another marker of inflammation in the kidney, Fsp1 (S100A4)[68,69], showed a similar pattern of increased expression with cyst formation and rapid resolution with PC2 re-expression in *Pkd2*$^{Cre/Flpo}$ mice (Supplementary Fig. 11b–g). Resolution of chemokine expression and macrophage infiltration follows the same rapid time course as reduction in kidney volume following re-expression of PC2-HA and supports a causal effect of absence or presence of polycystin on the presence or absence, respectively, of increased infiltration by monocytes in the kidney.

In addition to Mcp-1, the cytokines IL–6 and TNFα have been associated with inflammation in kidney injury and ADPKD[61,70]. Increased IL–6 is generally deleterious in acute and chronic kidney injury[71,72] and ADPKD[61,73] and may be a marker for systemic inflammation in a subset of ADPKD patients[74]. Whole kidney IL-6 mRNA expression was increased in cystic kidneys at 13, 14 and 16 weeks and was normalized in both 14 and 16 week

kidneys following PC2-HA re-expression (Supplementary Fig. 11h,i). The cytokine tumor necrosis factor-α (TNF-α) is elevated in human cyst fluid and its activity is associated with increased cyst growth in ADPKD model systems[75,76]. We found that TNF-α protein expression is significantly elevated in *Pkd2* knockout kidney tissue lysates at 13, 14 and 16 weeks age (Fig. 5e–h). PC2-HA re-expression beginning at 13 weeks normalized TNF-α to control levels in kidneys at 14 and 16 weeks (Fig. 5e,g). In the cystic tissues, TNF-α expression localized to a subset of cysts. It was largely absent from kidneys with PC2-HA re-expression (Fig. 5f,h). TNF-α can regulate expression of the NLRP3 inflammasome[77–79], and crystal deposition in the kidney, a known stimulus for activation of the NLRP3 inflammasome[80,81], has been proposed to accelerate polycystic kidney disease[82]. NLRP3 canonical inflammasomes activate caspase-1 by promoting autoproteolytic cleavage of pro-caspase-1. Active cleaved caspase-1 (p20) was significantly upregulated in kidney tissue lysates at 13, 14 and 16 weeks age in the *Pkd2* knockout kidneys; levels were normal at 14 and 16 weeks age following PC2-HA re-expression that was started at 13 weeks (Fig. 5i–l). Cleaved caspase-1 expression localized to a subset of cysts of both proximal and distal nephron origin at 14 and 16 weeks and was absent from kidneys with PC2-HA re-expression (Fig. 5j,l). In large measure, TNF-α and cleaved caspase-1 expression co-localized with regions of cystic kidneys showing significant infiltrates of F4/80 positive cells (Supplementary Fig. 12). These studies show a rapid and significant resolution of inflammatory changes associated with polycystic kidney disease in response to broad re-expression of PC2-HA. The rapid reversal of these biochemical and cellular changes suggest a causal association between polycystin function and the immediate stimuli for turning inflammatory responses on and off in ADPKD kidney tissue.

Effects of PC2 re-expression on fibrotic changes.

A hallmark of chronic kidney diseases including ADPKD is the occurrence of tubulointerstitial fibrosis characterized by accumulation of extracellular matrix proteins (ECM) and activation of myofibroblasts[16]. Whether these processes are secondary to the activity of infiltrating macrophages or more directly related to the loss of polycystins in cyst cells is uncertain[37,83–85]. We investigated whether abnormal ECM accumulation and myofibroblast activation reverse along with the other features of ADPKD upon re-expression of PC2-HA. Whole kidney mRNA expression of the ECM components *Col1a1*, *Col3a1* and *Fn1* (fibronectin) in 13, 14 and 16 week old cystic kidneys showed that expression of each gene was already elevated at 13 weeks and remained elevated in the cystic *Pkd2* knockouts at the later time points (Supplementary Fig. 13). Re-expression of PC2-HA beginning at 13 weeks resulted in normalization of expression for all three genes by 14 weeks (Supplementary Fig. 13). We examined the correlation of fibronectin protein expression with the transcript expression data by both immunoblotting and immunohistochemistry. Fibronectin protein was significantly elevated at 14 and 16 weeks in cystic kidneys but returned to baseline levels by 16 weeks with PC2 re-expression (Fig. 6a–d). Expression at 14 weeks appeared more variable in cystic kidneys and showed intermediate levels after re-expression, raising the possibility that the time course for resolution of fibronectin expression may be somewhat slower than other features of ADPKD. The extensive fragmentation of fibronectin seen in cystic kidneys may indicate activity of endopeptidases that cleave ECM components to foster tissue remodeling[86].

Finally, there was progressive myofibroblast activation in cystic kidneys as indicated by immunoblotting and immunohistochemistry for α-smooth muscle actin (α-SMA) and platelet derived growth factor receptor beta (PDGFRβ), and both were resolved after PC2 re-expression (Fig. 6e–l). Fibrosis manifest by ECM deposition and myofibroblast activation is reversible in vivo in a polycystin dependent manner in mouse models of ADPKD.

Late stage reversal of ADPKD.

The above studies examined the potential for reversing ADPKD with re-expression of PC2 in early stage disease. We next examined the effects of PC2 reactivation occurring at a more advanced stage of ADPKD in mice. *Pkd2*$^{Cre/Flpo}$ mice were again treated with doxycycline from P28–42 to inactivate *Pkd2*^{fl} and initiate cyst formation, but treatment with tamoxifen for 7 days was started at 16 weeks age to induce re-expression of PC2-HA at a more cystic stage. Mice were examined at 19 weeks of age (Fig. 7a–d and Supplementary Fig. 14). Sixteen-week-old mice show overall more severe polycystic kidney disease at the time of initiation of PC2 re-expression. At 19 weeks, mice without re-expression had a trend toward more severe structural kidney disease but were more notable for worsening kidney function as measured by BUN (Fig. 7a–d and Supplementary Fig. 14). When examined at 19 weeks, kidneys with re-expression of PC2 showed KW/BW ratios and CI not different from non-cystic animals and significantly lower compared to both 16 and 19 weeks cystic animals. Although BUNs tended to be lower than 19-week kidneys without re-expression, some of the mice have persistently impaired kidney function despite normalization of kidney size and cystic index. Histological examination confirmed the presence of severe cystic changes at 16 and 19 weeks in the absence of PC2-HA re-expression (Fig. 7e–g). Kidneys with re-expression had large areas of normal appearing tubules but also areas of residual fibrosis and tubular atrophy and areas of persistent inflammation (Fig. 7e–g). Overall, these findings are reminiscent of the findings described in the MRI study above for the very large kidney at 13 weeks, which had a reduction in kidney volume >6-fold but did not return to a normal BUN (Fig. 2e). The late stage reactivation studies show that kidney volume and structure, and specifically the presence of cysts, remain highly responsive to polycystin protein expression despite advanced disease. Kidney functional recovery is more variable and less complete likely because underlying scarring and fibrosis and nephron dropout is not reversible.

ADPKD due to *Pkd1* is reversible.

Finally, we tested whether the findings in ADPKD models based on *Pkd2* were also true of *Pkd1* using an analogous modified BAC transgenic re-expression model system (Supplementary Note). The *Pkd1*^{FSF} BAC transgene expressed FLAG and HA epitope tagged PC1 in a tamoxifen dependent manner when combined with *Rosa26*^{FlpoER} (Supplementary Fig. 15). We generated *Pkd1*$^{fl/—}$; *Pkd1*^{FSF}; *Pax8*^{rtTA}; *TetO*^{Cre}; *Rosa26*^{FlpoER} experimental mice, abbreviated *Pkd1*$^{Cre/Flpo}$. All study mice were hemizygous for *Pkd1*^{FSF}, *Pax8*^{rtTA} and *TetO*^{Cre}. Non-cystic controls were *Pkd1*$^{fl/—}$; *Pkd1*^{FSF}; *Rosa26*^{FlpoER} mice. All experimental and control mice received oral doxycycline from P28–42. This resulted in inactivation of *Pkd1*^{fl} in *Pkd1*$^{Cre/Flpo}$ mice, resulting in significantly increased KW/BW ratio and BUN at 16 weeks and increased CI at 13 and 16 weeks age (Fig. 8 and)Supplementary Fig. 16. This *Pkd1* model of ADPKD is fully penetrant but also has variable severity

including the previously reported sex dimorphism[87] (Supplementary Fig. 16). PC1 re-expression using *Pkd1*$^{Cre/Flpo}$ mice treated sequentially with doxycycline from P28–42 to inactivate *Pkd1*^{fl} followed by tamoxifen for 7 days beginning at 13 weeks age to induce re-expression resulted in resolution of the elevated KW/BW ratio and CI at 16 weeks when compared with 13 and 16 week-old mice without PC1 re-expression (Fig. 8a–d). Histological examination shows the presence of cystic dilations at 13 weeks prior to PC1 re-expression and progression of the polycystic disease at 16 weeks in the absence of PC1 re-expression. Following tamoxifen induced re-expression of PC1 beginning at 13 weeks, there is substantial histological resolution of kidney cysts, albeit with some persistent tubule dilation, at 16 weeks age (Fig. 8e). Polycystin-1, like polycystin-2, exerts dynamic bidirectional control of kidney structure in ADPKD mouse models. Based on the findings reported here, manifestations of ADPKD cannot only be slowed, but, under the correct circumstances, can be reversed. These findings suggest promise for the treatment of the human disease if the correct therapeutic strategy and timing of its application can be discovered and implemented.

Discussion

A major mechanism for initiating cyst formation in human ADPKD is somatic “second hit” mutations resulting in cellular recessive loss of *PKD1* or *PKD2* function on the respective germline heterozygous background. If one were to conceive of an “ideal” therapy after cysts had already formed, one could propose functional re-expression at physiological levels of the lost PKD gene. The current study examined the effect re-expression of ADPKD genes in mouse kidneys with pre-existing polycystic disease and in so doing also examined the capacity of the adult kidney for repair and regeneration. Re-expression of polycystins not only reversed presumed cell autonomous responses like alterations in epithelial cell shape, proliferation and autophagy, but also reversed changes at the level of the whole kidney including inflammation, ECM deposition and myofibroblast activation. The more advanced the stage of ADPKD at the time of re-expression, the less complete the resolution of the non-cell autonomous processes such as fibrosis and inflammation. Surprisingly, tubule and component cell morphology, which are more likely attributable to cell autonomous processes, still showed substantial capacity for reversal even at later stages of disease. The findings show that ADPKD is reversible in a stage-specific manner and that kidney tissues show a striking and unexpected capacity for structural plasticity. Polycystins exert a significant degree of dynamic control over structural and functional homeostasis in the adult kidney.

The fact that there are currently no molecularly defined precedents for pathways that can actively and reversibly remodel the adult kidney affirms the premise that the molecular processes that comprise polycystin signaling remain to be discovered. While most features we examined (e.g., cellular proliferation, inflammation, and ECM deposition) showed downregulation in response to polycystin re-expression, it is notable that autophagy showed increased activity in response to re-expression of polycystin. This raises the possibility of a role for enhanced autophagy in the reparative process in vivo. Several pathways that regulate autophagic flux including mammalian target of rapamycin (mTOR), AMP-activated protein kinase (AMPK) and sirtuins have been implicated in ADPKD[24,25,29–31,39].

There is evidence of impaired autophagic flux in ADPKD from in vitro data[88,89] and non-orthologous animal models[90], although a hypomorphic *Pkd1* mouse model failed to detect any differences in autophagic flux[91]. Outside of the kidney, studies in cardiac myocytes found that knockout of *Pkd2* suppressed activation of autophagic flux triggered by nutrient depletion in vivo[92]. We found similarly reduced autophagic flux in mouse kidneys under nutrient stress following loss of PC2 and showed that this was not only normalized, but was increased beyond baseline by re-expression of PC2. It may be hypothesized that enhanced autophagy following polycystin re-expression is a mechanism for constructive renewal and remodeling that returns tubule cells to more normal morphology and function as part of repairing ADPKD.

The findings support the hypothesis that the normal function of polycystins is the active maintenance and dynamic regulation of the three-dimensional structural organization and associated spatially determined function of the kidney. Our previous work showed that polycystins are negative regulators of cilia-dependent cyst activating (CDCA) signals, which in the setting of intact cilia lacking polycystins drive destructive remodeling of kidney tubules and result in ADPKD[46]. The current study suggests that polycystins are not simply a ‘brake’ on CDCA, but rather are part of a counterbalancing signal (i.e. ‘cruise control’) that dynamically maintains the nephron at structural and functional setpoints mediated by physiological inputs for which polycystins are the sensors. The physiological inputs to which polycystins respond remain unknown. Current hypotheses for the inputs regulating polycystin function include flow-dependent laminar shear stress[93] and ligand-mediated signaling (e.g.,[34,45]). Regardless of the input, the rapid reversal of multiple aspects of the ADPKD phenotype following re-expression of polycystins indicates that the input signals acting on polycystins to promote regeneration of normal cell and tubule morphology are retained despite the profound changes in cell shape, nephron morphology and interstitial responses present in cystic kidneys. This is, for example, consistent with a regulatory auto-ligand hypotheses for PC1[11,49]. More broadly, this finding is most consistent with polycystins responding to local inputs such as locally altered laminar shear stress patterns and local paracrine or autocrine factors.

Another feature of the findings is that cyst growth following loss of polycystin has a slower time course than polycystin-dependent repair. Following loss of polycystins, cyst growth and the associated changes take weeks or months in mouse models[5,46] and years or decades in the human disease. Reversal of the pleiotropic manifestations of ADPKD in mice requires only days or weeks. Although the time course or even the potential for repair in humans cannot be known until the relevant therapies are developed, if the biology in mice does translate to the orthologous processes in humans, then the rate of reversal in human ADPKD could be manifest in months or a few years rather than decades. This would suggest that a therapy that can achieve repair of human ADPKD may act over a shorter time than required for the disease to progress and could therefore be applied to ‘reset’ kidney size and function closer to baseline at intervals along patients’ clinical course. Clinical trials of such therapies may also require a shorter time to demonstrate efficacy than the serial image-based evaluation strategies currently used[22,94].

The expectations of therapeutic repair of ADPKD must be tempered by the observation that the degree to which these changes are substantially reversible depend on the stage of underlying disease severity at the time of intervention. As indicated by PC2 reactivation during later stage ADPKD, fibrosis and scarring at more advanced stages is no longer fully reparable even though the kidneys show substantial improvement in cyst burden and total kidney volume. Although kidney size appears more responsive to polycystin re-expression than kidney function in advanced disease, it is important to reserve making any conclusions regarding the relationship of kidney and cyst volume to kidney function following polycystin re-expression at this point. It will require the application of serial glomerular filtration rate (GFR) measurements and longer preclinical follow-up to determine whether or not there is significant improvement or stabilization of kidney function when the kidney volume decreases following polycystin gene re-expression. It is also important to reserve judgment as to the potential for repair in early versus late human ADPKD. The mouse models are based on synchronized inactivation of polycystins along large swaths of the nephron. The human disease is thought to occur by a more stochastic and focal second hit mechanism that should give rise to cysts that are distributed over a range of severities and focality within the kidney. In human ADPKD, significant cyst burden can still be associated with moderate impairment of GFR and with regions of the kidney with preserved architecture and function. Sufficiently early intervention with an agent fostering repair of the ADPKD kidney should enable improvement of cysts in those areas where the scarring has not progressed to the irreversible state. Under these circumstances, therapy directed at targets that have the potential to reverse the disease should be effective not only reducing cyst and kidney size, but may also be effective in delaying and even preventing progression to end stage kidney disease in ADPKD. This study provides evidence that an effective therapy directed at the molecular agents effecting the same molecular response as polycystin re-expression may not just slow kidney growth but may actively reduce kidney and cyst size and potentially stabilize or improve kidney function.

Methods

BAC modification.

We adapted published BAC recombineering technologies[95,96] to modify *Pkd2*- and *Pkd1*-containing BACs[18,97]. The brief method outlined for inserting the *FRT*-4XSTOP-*FRT* cassette into *Pkd2* was applied to all BAC modifications in this study. *Pkd2* BAC DNA was electroporated into DY380 bacteria, which have stably integrated a defective λ prophage containing the Red recombination genes *exo*, *bet* and *gam* under a strong pL promoter controlled by the temperature sensitive cI857 repressor (kind gift from Dr. Donald Court, National Cancer Institute). A recombination cassette was constructed by flanking a *rpsL*+-*kana* selection cassette (Addgene, #20871) with two short (~525 bp) homology arms from *Pkd2* intron 1. The same two homology arms were introduced to flank the *FRT*-4XSTOP-*FRT* (FSF) cassette in a plasmid in which *lox*-4XSTOP-*lox* was modified to FSF (Addgene, #11584). The *rpsL*+-*kana* cassette was introduced into *Pkd2* intron 1 region of the BAC after activation of the Red recombination system at 42 °C under positive selection by kanamycin resistance. The *rpsL*+-*kana* cassette in this intermediate was replaced by introducing *FRT*-4XSTOP-*FRT* cassette with *Pkd2* homology arms under negative selection

with streptomycin sensitivity conferred by the *rpsL*+ gene after the activation of the Red recombination system at 42 °C. The final *Pkd2*^{FSF} BAC containing the *FRT*-4XSTOP-*FRT* was shown to contain only the intended recombination and no other rearrangements using DNA restriction fingerprinting, direct sequencing and in vitro recombination in the SW105 bacterial strain carrying L-arabinose-inducible Flp gene as described in the Results. The above methods and validation steps were also used for making the *Pkd1*^{FSF} BAC.

Mouse strains and procedures.

Linearized modified BAC DNA purified by CHEF electrophoresis was used for pronuclear injection to generate transgenic founder lines. The BAC transgenic lines were produced in the Yale Genome Editing Center in (C57BL/6J X SJL/J) F2 zygotes. Founders were identified by PCR genotyping, verified by sequencing of PCR products and BAC copy number was determined by genomic quantitative PCR as described previously[18,97]. The *Pkd2*^{FSF} BAC founder used in the current study has two copies of the BAC transgene. Three *Pkd1*^{FSF} BAC founders with BAC copy numbers 1, 4 or 8, respectively, were used in this study. All strains were backcrossed at least four generations with C57BL/6J and are therefore expected to be at least 90% C57BL/6J congenic. Mice of both sexes were used. Mice were examined at 10 weeks, 13 weeks, 14 weeks, 16 weeks, or 19 weeks of age as specified in the text. All animals were maintained in secure, intact, clean, fully assembled, bar coded, static micro-isolator cages. Temperature was maintained between 68–79 °F and humidity between 30–70% with 12:12 light:dark cycles. The other mouse strains used in the current study have been previously described (*Pkd2*^{flox}, *Pkd2*$^{-}$, *Pkd1*^{flox}, *Pkd1*$^{-}$, *Pax8*^{rtTA}, *TetO*^{Cre}, *UBC*^{CreER})[46]. The *Rosa*^{FlpoER} (ref. 50) was a kind gift from Dr. Alexandra Joyner (Memorial Sloan Kettering, NYC). All animals were used in accordance with scientific, humane, and ethical principles and in compliance with regulations approved by the Yale University Institutional Animal Care and Use Committee (IACUC).

Gene inactivation in the *Pax8*^{rtTA}*; TetO*^{Cre} models was induced with 2 mg/ml doxycycline in drinking water supplemented with 3% sucrose provided for 2 weeks from P28 to P42. Gene re-expression with *Rosa*^{FlpoER} was induced with tamoxifen 20 mg/ml in sunflower seed oil delivered by intraperitoneal injection at a dose of 0.1 mg/g/day for 7 days beginning at 13 or 16 weeks of age as indicated. Mice were euthanized at 10 weeks, 13 weeks, 14 weeks, 16 weeks, and/or 19 weeks of age. Gene inactivation in the *UBC*^{CreER} models was induced with intraperitoneal tamoxifen given for 7 days beginning at post-natal day 28. Mice were euthanized by standard protocols approved by Yale IACUC. Blood was collected by ventricular puncture. Sera were separated using Plasma Separator Tubes with lithium heparin. Serum urea nitrogen was analyzed by the George M. O'Brien Kidney Center at Yale. One kidney was snap-frozen for protein and mRNA extraction, and another kidney was fixed in situ by perfusion through the heart with 4% paraformaldehyde in 1 x PBS for hematoxylin and eosin, Masson's trichrome and immunohistochemistry.

Magnetic resonance imaging acquisition and kidney volume data processing.

All scans were acquired on a 4T horizontal-bore Bruker spectrometer (Billerica, MA, USA) using a ^{1}H RF volume coil of 4-cm diameter. MRI images were obtained using a 3D gradient-echo (GE) sequence with a resolution of 256×128×64, a field of view (FOV) of

32 mm × 25.6 mm × 25.6 mm, a repetition time (TR) of 70 ms, an echo time (TE) of 4 ms and a flip angle of 30°. To minimize the movement artefacts induced by the breathing, the acquisition was triggered using an MRI compatible small animal monitoring and gating system (SA Instruments, Inc., Stony Brook, NY, USA). The left and right kidney volumes were measured using BioImage Suite (version 3.01; http://www.bioimagesuite.org/) by manually selecting the region of interest (ROI) corresponding to each kidney in each slice. These two ROIs provided a 3D representation of the two kidneys, and the volume of each kidney was calculated by multiplying the volume of a voxel (0.01 mm^3) with the number of voxels in each ROI. Volume measurements were done blinded to mouse genotype and treatment. All experiments were performed according to NIH guidelines and in accordance with Yale University IACUC guidelines and procedures.

Immunohistochemistry.

Cryosections (5–7 μm) were used for immunofluorescent studies according to standard procedures. The following antibodies and lectins were used: rat anti-HA (1:200, 11867423001, Roche); FITC (FL-1031) or rhodamine (RL-1032) conjugated-Dolichos biflorus agglutinin (1:50, DBA, Vectors Laboratories); FITC-Lotus tetragonolobus agglutinin (1:200, LTA, FL-1321, Vectors Laboratories); rabbit anti-megalin (1:500)[98]; sheep-anti-Tamm-Horsfall protein (1:300, AB733, MilliporeSigma); mouse anti-cleaved caspase-1 (p20) (1:200, AG-20B-0042-C100, Adipogen International); mouse anti-TNFα (1:200, SC-52746, Santa Cruz Biotechnology); rabbit anti-fibronectin (1:500, AB2033, MilliporeSigma); rabbit anti-alpha smooth muscle actin (1:200, ab5694, Abcam); rabbit anti-PDGF receptor beta (1:200, AB32570, Abcam); rat anti-F4/80 (1:200, MCA497R, AbD Serotec); rat anti-laminin gamma 1, clone A5 (1:100, MAB1914P, EMD Millipore Corp.); rabbit anti-LC3-II (1:200, 2775S, Cell Signaling Technology); rabbit antibody to PC2 (YCC2; 1:2,000)[99]; chicken anti-GFP (1:200, GFP-1020, Aves labs); Alexa-488, Alexa-594 and Alexa-647 conjugated secondary antibodies (Molecular Probes). Hoechst 33342 (DAPI, H-3570, Molecular Probes) was used for nuclear staining. Hematoxylin solution Gill no. 3 was used for nuclear counterstaining. PC2-HA expression in kidney was detected using paraffin sections and DAB peroxidase substrate kit (SK-4100, Vector Laboratories, Inc.) with rat anti-HA antibody (1:200, 11867423001, Roche). Cystic index was calculated using frontal plane sections of kidneys processed for hematoxylin and eosin and scanned by light microscopy and processed under the control of MetaMorph software (version 7.7; Universal Imaging) as previously reported[46].

Proliferation assay.

Proliferation was measured by EdU-positive nuclei and Ki67-positive nuclei. For EdU incorporation, mice received 50 mg/kg body weight of 5-ethynyl-2'-deoxyuridine (EdU, A10044, Invitrogen) by intraperitoneal injection 4 hours before euthanasia. Kidneys were fixed with 4% PFA overnight and embedded in OCT after 30% sucrose infiltration and processed for immunofluorescence. EdU staining was performed with Click-iT™ EdU Alexa Fluor™ 594 Imaging Kit (C10339, Invitrogen) and Click-iT™ EdU Alexa Fluor™ 488 Imaging Kit (C10337, Invitrogen). Ki67 expression in kidney was detected with rabbit anti-Ki67 antibody (1:300, RM-9106-S1, Thermo Scientific). Numbers of EdU and Ki67 positive nuclei were counted amongst at least 1,000 DBA or LTA positive nuclei per animal.

Protein preparation, immunoblotting and quantitation by densitometry.

Frozen whole kidneys were homogenized with ice-cold Hanoka's IP buffer (150 mM NaCl, 20 mM NaH_2PO_4, 10% glycerol, 0.5% Triton X-100) or RIPA Buffer (140 mM NaCl, 10 mM Tris-HCl pH 8.0, 1 mM EDTA, 0.5 mM EGTA, 1% Triton X-100, 0.1% SDS and 0.1% Na-deoxycholate) supplemented with complete EDTA-free protease inhibitor cocktail tablets (Roche) and PhosSTOP phosphatase inhibitor cocktail tablets (Roche). Lysates were centrifuged for 10,000 x *g* for 10 min at 4 °C. Protein concentrations were measured with Protein Assay Dye Reagent Concentrate (5000006, Bio-Rad). Equal amounts of total protein were loaded and separated in 4–20% Mini-Protean TGX Precast Gels (4568094, Bio-Rad) or 3–8% NuPAGE Novex Tris-Acetate Gels (EA0375BOX, Invitrogen) and transferred to Immobilon-P PVDF Membrane (IPVH00010, MilliporeSigma). Membranes were sequentially incubated with primary antibodies overnight at 4 °C after 1 hour blocking with 5% milk. In addition to those previously listed, primary antibodies used: rat anti-HA (1:3,000, 11867423001, Roche); rabbit anti-Flag antibody (1:3,000, F7425, MilliporeSigma); rabbit anti-Cyclin D1 (1:1,500, AB134175, Abcam); rabbit anti-cleaved caspase-3 (1:1,500, 9664S, Cell Signaling Technology); mouse anti-cleaved Parp (1:1,500, 5625S, Cell Signaling Technology); rabbit anti-S100A4 (Fsp1, 1:1,000, ab197896, Abcam); rabbit anti-LC3-II (1:2,000, 2775S, Cell Signaling Technology); rabbit anti-Hsp90 (1:3,000, 4877S, Cell Signaling Technology); rabbit antibody to PC2 (YCC2; 1:10,000)[99]; rabbit anti-Gapdh (1:3,000, 2118S, Cell Signaling Technology). Secondary antibodies anti-rabbit-HRP, anti-rat-HRP and anti-mouse-HRP (1:5,000, Jackson ImmunoResearch Laboratories) were incubated with the membrane for 1 hour. Immunoprecipitation was done with monoclonal anti-HA-Agarose antibody (A2095–1ML, MilliporeSigma). The images were acquired with Odyssey Fc Imaging System (LI-COR Biosciences), and the analysis and quantitation of individual immunoblot bands was performed with Image Studio Lite Western Blot Analysis software (LI-COR Biosciences).

RNA isolation, RT-PCR and quantitative RT-PCR (qPCR).

Total RNA was isolated from mouse kidney tissue using RNeasy Mini Kit (74104, Qiagen), and used for cDNA synthesis using SuperScript II Reverse Transcriptase (18064022, Invitrogen). qPCR was performed using iTaq Universal SYBR green Supermix (1725122, Bio-Rad) and analyzed by CFX system (Bio-Rad). The primers were used for quantifying mRNA expression in mouse kidneys are provided in Supplementary Table 2.

Sample size, power calculations and statistics.

Sample size and power calculations were performed prospectively using STPLAN (ver. 4.5; University of Texas, MD Anderson Cancer Center). Calculations were based on the following inputs: We selected a significance level (α) as 0.05 (one sided) and 0.80 power (1 - β) as our threshold. The kidney weight-to-body weight ratio (KW/BW) mean 13.4% with s.d. of ± 6.97% was empirically derived from our observed data in $Pkd2^{fl/-}$; $Pkd2^{FSF}$; $Pax8^{rtTA}$; $TetO^{Cre}$; $Rosa26^{FlpoER}$ mice at 16 weeks age after receiving oral doxycycline from P28–42. Our alternative hypothesis was that *Pkd2* re-expression mice would result in at least a 40% decrease in the KW/BW ratio. Under these expectations, 12 mice could achieve 80% power to detect the difference between the null hypothesis and the alternative hypothesis.

Most of the quantitative data was analyzed by one-way ANOVA followed by Tukey's multiple-comparison test using GraphPad Prism 8.3.0 software. The data of Figure 1j were analyzed using Sigmoidal dose-response (variable slope) nonlinear regression. The data of Figure 2c were analyzed using two-way ANOVA followed by Tukey's multiple comparison test. The comparison of two groups in Supplementary Figure 5 was performed using the two-tailed unpaired *t*-test. The data in Supplementary Figure 6d were analyzed by one tailed nonparametric Spearman correlation and the 95% confidence interval plotted by simple linear regression. All data are presented as mean ± s.e.m. $P < 0.05$ was considered the threshold for significance throughout. Exact P values are provided for all $P > 0.0001$.

Data Availability

There are no accession codes, unique identifiers, or weblinks for publicly available datasets associated with this publication. The figures do not have associated raw data. There are no restrictions on data availability associated with any part of this work. Full-length immunoblots supporting all the figures are provided as data source files.

Supplementary Material

Refer to Web version on PubMed Central for supplementary material.

Acknowledgements

We thank the George M. O'Brien Kidney Center at Yale (P30 DK079310) for assistance with BAC recombineering and BUN measurements. This work was supported by NIH/NIDDK grants R01 DK121948 and RC1 DK086738 to S. S. and a PKD Foundation grant (196F14a) to M.M. We are grateful for the generous and steadfast support from the Amy P. Goldman Foundation.

References

1. Harris PC & Torres VE Genetic mechanisms and signaling pathways in autosomal dominant polycystic kidney disease. J. Clin. Invest. 124, 2315–2324 (2014). [PubMed: 24892705]
2. Qian F, Watnick TJ, Onuchic LF & Germino GG The molecular basis of focal cyst formation in human autosomal dominant polycystic kidney disease type I. Cell 87, 979–987 (1996). [PubMed: 8978603]
3. Wu G et al. Somatic inactivation of Pkd2 results in polycystic kidney disease. Cell 93, 177–188 (1998). [PubMed: 9568711]
4. Leonhard WN, Happe H & Peters DJ Variable cyst development in autosomal dominant polycystic kidney disease: the biologic context. J. Am. Soc. Nephrol. 27, 3530–3538 (2016). [PubMed: 27493259]
5. Piontek K, Menezes LF, Garcia-Gonzalez MA, Huso DL & Germino GG A critical developmental switch defines the kinetics of kidney cyst formation after loss of Pkd1. Nat. Med. 13, 1490–1495 (2007). [PubMed: 17965720]
6. Lantinga-van Leeuwen IS et al. Kidney-specific inactivation of the Pkd1 gene induces rapid cyst formation in developing kidneys and a slow onset of disease in adult mice. Hum. Mol. Genet. 16, 3188–3196 (2007). [PubMed: 17932118]
7. Davenport JR et al. Disruption of intraflagellar transport in adult mice leads to obesity and slow-onset cystic kidney disease. Curr. Biol. 17, 1586–1594 (2007). [PubMed: 17825558]
8. Takakura A et al. Renal injury is a third hit promoting rapid development of adult polycystic kidney disease. Hum. Mol. Genet. 18, 2523–2531 (2009). [PubMed: 19342421]
9. Patel V et al. Acute kidney injury and aberrant planar cell polarity induce cyst formation in mice lacking renal cilia. Hum. Mol. Genet. 17, 1578–1590 (2008). [PubMed: 18263895]

10. Bastos AP et al. Pkd1 haploinsufficiency increases renal damage and induces microcyst formation following ischemia/reperfusion. J. Am. Soc. Nephrol. 20, 2389–2402 (2009). [PubMed: 19833899]
11. Formica C & Peters DJM Molecular pathways involved in injury-repair and ADPKD progression. Cell Signal. 72, 109648 (2020). [PubMed: 32320858]
12. Karihaloo A et al. Macrophages promote cyst growth in polycystic kidney disease. J. Am. Soc. Nephrol. 22, 1809–1814 (2011). [PubMed: 21921140]
13. Chen L et al. Macrophage migration inhibitory factor promotes cyst growth in polycystic kidney disease. J. Clin. Invest. 125, 2399–2412 (2015). [PubMed: 25961459]
14. Swenson-Fields KI et al. Macrophages promote polycystic kidney disease progression. Kidney Int. 83, 855–864 (2013). [PubMed: 23423256]
15. Cassini MF et al. Mcp1 promotes macrophage-dependent cyst expansion in autosomal dominant polycystic kidney disease. J. Am. Soc. Nephrol. 29, 2471–2481 (2018). [PubMed: 30209078]
16. Song CJ, Zimmerman KA, Henke SJ & Yoder BK Inflammation and fibrosis in polycystic kidney disease. Results Probl. Cell Differ. 60, 323–344 (2017). [PubMed: 28409351]
17. Cornec-Le Gall E et al. Type of PKD1 mutation influences renal outcome in ADPKD. J. Am. Soc. Nephrol. 24, 1006–1013 (2013). [PubMed: 23431072]
18. Fedeles SV et al. A genetic interaction network of five genes for human polycystic kidney and liver diseases defines polycystin-1 as the central determinant of cyst formation. Nat. Genet. 43, 639–647 (2011). [PubMed: 21685914]
19. Hopp K et al. Functional polycystin-1 dosage governs autosomal dominant polycystic kidney disease severity. J. Clin. Invest. 122, 4257–4273 (2012). [PubMed: 23064367]
20. Walz G et al. Everolimus in patients with autosomal dominant polycystic kidney disease. N. Engl. J. Med. 363, 830–840 (2010). [PubMed: 20581392]
21. Serra AL et al. Sirolimus and kidney growth in autosomal dominant polycystic kidney disease. N. Engl. J. Med. 363, 820–829 (2010). [PubMed: 20581391]
22. Torres VE et al. Tolvaptan in patients with autosomal dominant polycystic kidney disease. N. Engl. J. Med. 367, 2407–2418 (2012). [PubMed: 23121377]
23. Torres VE et al. Tolvaptan in later-stage autosomal dominant polycystic kidney disease. N. Engl. J. Med. 377, 1930–1942 (2017). [PubMed: 29105594]
24. Calvet JP The role of calcium and cyclic AMP in PKD. in Polycystic Kidney Disease (ed. Li X) (Brisbane (AU), 2015).
25. Kakade VR et al. A cAMP and CREB-mediated feed-forward mechanism regulates GSK3beta in polycystic kidney disease. J. Mol. Cell. Biol. 8, 464–476 (2016). [PubMed: 27190311]
26. Parnell SC et al. A mutation affecting polycystin-1 mediated heterotrimeric G-protein signaling causes PKD. Hum. Mol. Genet. 27, 3313–3324 (2018). [PubMed: 29931260]
27. Zhang B, Tran U & Wessely O Polycystin 1 loss of function is directly linked to an imbalance in G-protein signaling in the kidney. Development 145, dev158931 (2018). [PubMed: 29530879]
28. Tsiokas L Function and regulation of TRPP2 at the plasma membrane. Am. J. Physiol. Renal Physiol. 297, F1–F9 (2009). [PubMed: 19244406]
29. Kipp KR et al. Comparison of folate-conjugated rapamycin versus unconjugated rapamycin in an orthologous mouse model of polycystic kidney disease. Am. J. Physiol. Renal Physiol. 315, F395–F405 (2018). [PubMed: 29717938]
30. Fantus D, Rogers NM, Grahammer F, Huber TB & Thomson AW Roles of mTOR complexes in the kidney: implications for renal disease and transplantation. Nat. Rev. Nephrol. 12, 587–609 (2016). [PubMed: 27477490]
31. Shillingford JM, Piontek KB, Germino GG & Weimbs T Rapamycin ameliorates PKD resulting from conditional inactivation of Pkd1. J. Am. Soc. Nephrol. 21, 489–497 (2010). [PubMed: 20075061]
32. DeCaen PG, Delling M, Vien TN & Clapham DE Direct recording and molecular identification of the calcium channel of primary cilia. Nature 504, 315–318 (2013). [PubMed: 24336289]
33. Delling M, DeCaen PG, Doerner JF, Febvay S & Clapham DE Primary cilia are specialized calcium signalling organelles. Nature 504, 311–314 (2013). [PubMed: 24336288]

34. Ha K et al. The heteromeric PC-1/PC-2 polycystin complex is activated by the PC-1 N-terminus. Elife 9, e60684 (2020). [PubMed: 33164752]
35. Harskamp LR, Gansevoort RT, van Goor H & Meijer E The epidermal growth factor receptor pathway in chronic kidney diseases. Nat. Rev. Nephrol. 12, 496–506 (2016). [PubMed: 27374915]
36. Bukanov NO et al. CDK inhibitors R-roscovitine and S-CR8 effectively block renal and hepatic cystogenesis in an orthologous model of ADPKD. Cell Cycle 11, 4040–4046 (2012). [PubMed: 23032260]
37. Lee K, Boctor S, Barisoni LM & Gusella GL Inactivation of integrin-beta1 prevents the development of polycystic kidney disease after the loss of polycystin-1. J. Am. Soc. Nephrol. 26, 888–895 (2015). [PubMed: 25145933]
38. Raman A et al. Integrin-linked kinase signaling promotes cyst growth and fibrosis in polycystic kidney disease. J. Am. Soc. Nephrol. 28, 2708–2719 (2017). [PubMed: 28522687]
39. Li X Epigenetics in ADPKD: understanding mechanisms and discovering treatment. in Polycystic Kidney Disease (ed. Li X) (Brisbane (AU), 2015).
40. Chang MY & Ong ACM Targeting new cellular disease pathways in autosomal dominant polycystic kidney disease. Nephrol. Dial. Transplant. 33, 1310–1316 (2017).
41. Rowe I et al. Defective glucose metabolism in polycystic kidney disease identifies a new therapeutic strategy. Nat. Med. 19, 488–493 (2013). [PubMed: 23524344]
42. Chiaravalli M et al. 2-deoxy-d-glucose ameliorates PKD progression. J. Am. Soc. Nephrol. 27, 1958–1969 (2016). [PubMed: 26534924]
43. Padovano V, Podrini C, Boletta A & Caplan MJ Metabolism and mitochondria in polycystic kidney disease research and therapy. Nat. Rev. Nephrol. 14, 678–687 (2018). [PubMed: 30120380]
44. Flowers EM et al. Lkb1 deficiency confers glutamine dependency in polycystic kidney disease. Nat. Commun. 9, 814 (2018). [PubMed: 29483507]
45. Kim S et al. The polycystin complex mediates Wnt/Ca(2+) signalling. Nat. Cell Biol. 18, 752–764 (2016). [PubMed: 27214281]
46. Ma M, Tian X, Igarashi P, Pazour GJ & Somlo S Loss of cilia suppresses cyst growth in genetic models of autosomal dominant polycystic kidney disease. Nat. Genet. 45, 1004–1012 (2013). [PubMed: 23892607]
47. Takiar V & Caplan MJ Polycystic kidney disease: pathogenesis and potential therapies. Biochim. Biophys. Acta 1812, 1337–1343 (2011). [PubMed: 21146605]
48. Avasthi P, Maser RL & Tran PV Primary cilia in cystic kidney disease. in Kidney Development and Disease (ed. Miller RK) 281–321 (Springer International Publishing, Cham, 2017).
49. Ma M, Gallagher AR & Somlo S Ciliary mechanisms of cyst formation in polycystic kidney disease. Cold Spring Harb. Perspect. Biol. 9, a028209 (2017). [PubMed: 28320755]
50. Lao Z, Raju GP, Bai CB & Joyner AL MASTR: a technique for mosaic mutant analysis with spatial and temporal control of recombination using conditional floxed alleles in mice. Cell Rep. 2, 386–396 (2012). [PubMed: 22884371]
51. Zhang M & Kirsch DG The generation and characterization of novel Col1a1FRT-Cre-ER-T2-FRT and Col1a1FRT-STOP-FRT-Cre-ER-T2 mice for sequential mutagenesis. Dis. Model Mech. 8, 1155–66 (2015). [PubMed: 26183214]
52. Nishio S et al. Pkd1 regulates immortalized proliferation of renal tubular epithelial cells through p53 induction and JNK activation. J. Clin. Invest. 115, 910–918 (2005). [PubMed: 15761494]
53. Thomson RB et al. Histopathological analysis of renal cystic epithelia in the Pkd2WS25/− mouse model of ADPKD. Am. J. Physiol. Renal Physiol. 285, F870–F880 (2003). [PubMed: 12851251]
54. Stroope A et al. Hepato-renal pathology in Pkd2ws25/− mice, an animal model of autosomal dominant polycystic kidney disease. Am. J. Pathol. 176, 1282–1291 (2010). [PubMed: 20093497]
55. Mizushima N & Komatsu M Autophagy: renovation of cells and tissues. Cell 147, 728–741 (2011). [PubMed: 22078875]
56. Tang C, Livingston MJ, Liu Z & Dong Z Autophagy in kidney homeostasis and disease. Nat. Rev. Nephrol. 16, 489–508 (2020). [PubMed: 32704047]

57. Shibazaki S et al. Cyst formation and activation of the extracellular regulated kinase pathway after kidney specific inactivation of Pkd1. Hum. Mol. Genet. 17, 1505–1516 (2008). [PubMed: 18263604]
58. Torres JA et al. Ketosis ameliorates renal cyst growth in polycystic kidney disease. Cell Metab. 30, 1007–1023.e5 (2019). [PubMed: 31631001]
59. Fragiadaki M et al. STAT5 drives abnormal proliferation in autosomal dominant polycystic kidney disease. Kidney Int. 91, 575–586 (2017). [PubMed: 28104302]
60. Zerjatke T et al. Quantitative cell cycle analysis based on an endogenous all-in-one reporter for cell tracking and classification. Cell Rep. 19, 1953–1966 (2017). [PubMed: 28564611]
61. Li LX et al. Lysine methyltransferase SMYD2 promotes cyst growth in autosomal dominant polycystic kidney disease. J. Clin. Invest. 127, 2751–2764 (2017). [PubMed: 28604386]
62. Zhang C et al. Cyclin-dependent kinase 1 activity is a driver of cyst growth in polycystic kidney disease. J. Am. Soc. Nephrol. 32, 41–51 (2021). [PubMed: 33046531]
63. Zimmerman KA, Hopp K & Mrug M Role of chemokines, innate and adaptive immunity. Cell Signal. 73, 109647 (2020). [PubMed: 32325183]
64. Zheng D et al. Urinary excretion of monocyte chemoattractant protein-1 in autosomal dominant polycystic kidney disease. J. Am. Soc. Nephrol. 14, 2588–2595 (2003). [PubMed: 14514736]
65. Grantham JJ et al. Tolvaptan suppresses monocyte chemotactic protein-1 excretion in autosomal-dominant polycystic kidney disease. Nephrol. Dial. Transplant. 32, 969–975 (2017). [PubMed: 27190355]
66. Lannoy M et al. The positive effect of selective prostaglandin E2 receptor EP2 and EP4 blockade on cystogenesis in vitro is counteracted by increased kidney inflammation in vivo. Kidney Int. 98, 404–419 (2020). [PubMed: 32622526]
67. Lakhia R et al. Interstitial microRNA miR-214 attenuates inflammation and polycystic kidney disease progression. JCI Insight 5, e133785 (2020).
68. Le Hir M, Hegyi I, Cueni-Loffing D, Loffing J & Kaissling B Characterization of renal interstitial fibroblast-specific protein 1/S100A4-positive cells in healthy and inflamed rodent kidneys. Histochem. Cell Biol. 123, 335–346 (2005). [PubMed: 15856273]
69. Österreicher CH et al. Fibroblast-specific protein 1 identifies an inflammatory subpopulation of macrophages in the liver. Proc. Natl. Acad. Sci. USA 108, 308–313 (2011). [PubMed: 21173249]
70. Jo SK, Sung SA, Cho WY, Go KJ & Kim HK Macrophages contribute to the initiation of ischaemic acute renal failure in rats. Nephrol. Dial. Transplant. 21, 1231–1239 (2006). [PubMed: 16410269]
71. Durlacher-Betzer K et al. Interleukin-6 contributes to the increase in fibroblast growth factor 23 expression in acute and chronic kidney disease. Kidney Int. 94, 315–325 (2018). [PubMed: 29861060]
72. Kielar ML et al. Maladaptive role of IL-6 in ischemic acute renal failure. J. Am. Soc. Nephrol. 16, 3315–3325 (2005). [PubMed: 16192425]
73. Ravichandran K, Zafar I, Ozkok A & Edelstein CL An mTOR kinase inhibitor slows disease progression in a rat model of polycystic kidney disease. Nephrol. Dial. Transplant. 30, 45–53 (2015). [PubMed: 25239638]
74. Menon V et al. Inflammation, oxidative stress, and insulin resistance in polycystic kidney disease. Clin. J. Am. Soc. Nephrol. 6, 7–13 (2011). [PubMed: 20829421]
75. Li X et al. A tumor necrosis factor-alpha-mediated pathway promoting autosomal dominant polycystic kidney disease. Nat. Med. 14, 863–868 (2008). [PubMed: 18552856]
76. Zhou JX, Fan LX, Li X, Calvet JP & Li X TNFalpha signaling regulates cystic epithelial cell proliferation through Akt/mTOR and ERK/MAPK/Cdk2 mediated Id2 signaling. PLoS One 10, e0131043 (2015). [PubMed: 26110849]
77. McGeough MD et al. TNF regulates transcription of NLRP3 inflammasome components and inflammatory molecules in cryopyrinopathies. J. Clin. Invest. 127, 4488–4497 (2017). [PubMed: 29130929]
78. Jain N, Sudhakar C & Swarup G Tumor necrosis factor-alpha-induced caspase-1 gene expression. Role *of p73. FEBS J.* 274, 4396–4407 (2007). [PubMed: 17725714]

79. Alvarez S & Munoz-Fernandez MA TNF-alpha may mediate inflammasome activation in the absence of bacterial infection in more than one way. PLoS One 8, e71477 (2013). [PubMed: 23940760]
80. Mulay SR et al. Calcium oxalate crystals induce renal inflammation by NLRP3-mediated IL-1beta secretion. J. Clin. Invest. 123, 236–246 (2013). [PubMed: 23221343]
81. Knauf F et al. NALP3-mediated inflammation is a principal cause of progressive renal failure in oxalate nephropathy. Kidney Int. 84, 895–901 (2013). [PubMed: 23739234]
82. Torres JA et al. Crystal deposition triggers tubule dilation that accelerates cystogenesis in polycystic kidney disease. J. Clin. Invest. 130, 4506–4522 (2019).
83. Mangos S et al. The ADPKD genes pkd1a/b and pkd2 regulate extracellular matrix formation. Dis. Model Mech. 3, 354–365 (2010). [PubMed: 20335443]
84. Hassane S et al. Elevated TGFbeta-Smad signalling in experimental Pkd1 models and human patients with polycystic kidney disease. J. Pathol. 222, 21–31 (2010). [PubMed: 20549648]
85. Dwivedi N et al. Epithelial vasopressin type-2 receptors regulate myofibroblasts by a YAP-CCN2-dependent mechanism in polycystic kidney disease. J. Am. Soc. Nephrol. 31, 1697–1710 (2020). [PubMed: 32554753]
86. Bonnans C, Chou J & Werb Z Remodelling the extracellular matrix in development and disease. Nat. Rev. Mol. Cell Biol. 15, 786–801 (2014). [PubMed: 25415508]
87. Menezes LF, Lin CC, Zhou F & Germino GG Fatty acid oxidation is impaired in an orthologous mouse model of autosomal dominant polycystic kidney disease. EBioMedicine 5, 183–192 (2016). [PubMed: 27077126]
88. Zhu P, Sieben CJ, Xu X, Harris PC & Lin X Autophagy activators suppress cystogenesis in an autosomal dominant polycystic kidney disease model. Hum. Mol. Genet. 26, 158–172 (2017). [PubMed: 28007903]
89. Peintner L et al. Loss of PKD1/polycystin-1 impairs lysosomal activity in a CAPN (calpain)-dependent manner. Autophagy doi: 10.1080/15548627.2020.1826716 (2020).
90. Belibi F et al. Hypoxia-inducible factor-1alpha (HIF-1alpha) and autophagy in polycystic kidney disease (PKD). Am. J. Physiol. Renal Physiol. 300, F1235–F1243 (2011). [PubMed: 21270095]
91. Chou LF et al. Effect of trehalose supplementation on autophagy and cystogenesis in a mouse model of polycystic kidney disease. Nutrients 11, 42 (2018).
92. Criollo A et al. Polycystin-2-dependent control of cardiomyocyte autophagy. J. Mol. Cell. Cardiol. 118, 110–121 (2018). [PubMed: 29518398]
93. Praetorius HA The primary cilium as sensor of fluid flow: new building blocks to the model. A review in the theme: cell signaling: proteins, pathways and mechanisms. Am. J. Physiol. Cell Physiol. 308, C198–C208 (2015). [PubMed: 25428884]
94. Grantham JJ et al. Volume progression in polycystic kidney disease. N. Engl. J. Med. 354, 2122–2130 (2006). [PubMed: 16707749]
95. Wang S, Zhao Y, Leiby M & Zhu J A new positive/negative selection scheme for precise BAC recombineering. Mol. Biotechnol. 42, 110–116 (2009). [PubMed: 19160076]
96. Warming S, Costantino N, Court DL, Jenkins NA & Copeland NG Simple and highly efficient BAC recombineering using galK selection. Nucleic Acids Res. 33, e36 (2005). [PubMed: 15731329]
97. Cai Y et al. Altered trafficking and stability of polycystins underlie polycystic kidney disease. J. Clin. Invest. 124, 5129–5144 (2014). [PubMed: 25365220]
98. Zou Z et al. Linking receptor-mediated endocytosis and cell signaling: evidence for regulated intramembrane proteolysis of megalin in proximal tubule. J. Biol. Chem. 279, 34302–34310 (2004). [PubMed: 15180987]
99. Cai Y et al. Identification and characterization of polycystin-2, the PKD2 gene product. J. Biol. Chem. 274, 28557–28565 (1999). [PubMed: 10497221]

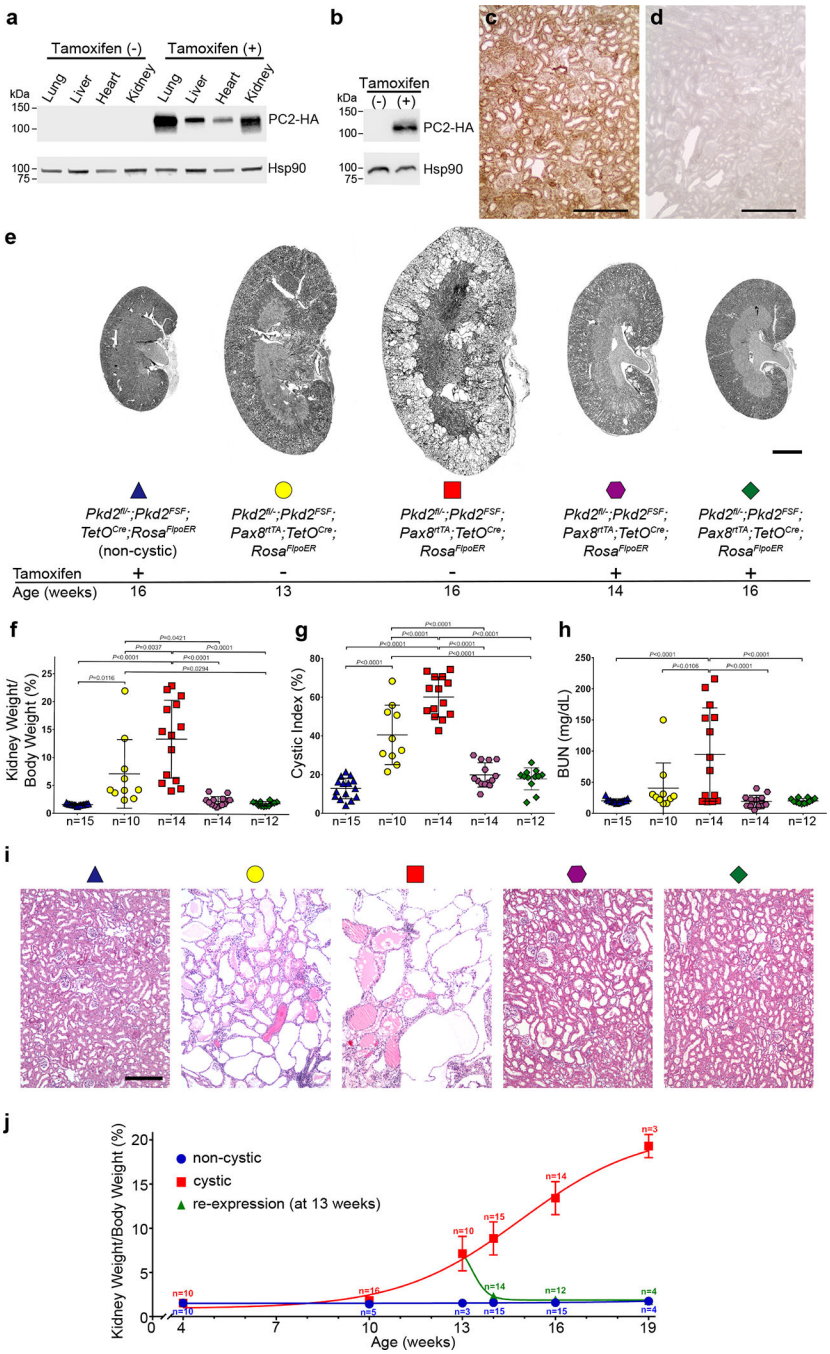

Figure 1 |. Reactivation of *Pkd2* reverses cyst formation.

a, PC2-HA expression detected by anti-HA immunoblotting of multiple tissue lysates at 16 weeks age from *Pkd2*$^{fl/—}$; *Pkd2*^{FSF}; *Pax8*^{rtTA}; *TetO*^{Cre}; *Rosa*^{FlpoER} (“*Pkd2*$^{Cre/Flpo}$”) treated either only with oral doxycycline from P28-P42 (tamoxifen (−)) or followed by tamoxifen (+) for 7 days beginning at 13 weeks age. Expression of PC2-HA only occurs in mice that received tamoxifen. **b**, Kidney lysates from mice with the same genotype and treatment as **a** but examined at 14 weeks age showing PC-HA expression within 1 week after starting tamoxifen (+). Experiments in **a** and **b** were done 3 times, each with tissue lysates from

different mice. **c,d**, Immunohistochemistry using anti-HA antibody with DAB staining in kidney sections from 16-week-old mice with the genotypes in **a** showing diffuse PC2-HA expression (brown) following tamoxifen induction (**c**) and absence of PC2-HA expression without tamoxifen induction (**d**). Experiments in **c** and **d** were done 3 times, each with tissue sections from different mice. Scale bar, 200 μm. **e**, Representative images of kidneys from mice with the indicated genotypes and ages. All mice received doxycycline (P28–42). Tamoxifen was administered daily for 7 days beginning at 13 weeks age to induce *Pkd2* re-expression in the groups indicated (+). Scale bar, 2 mm. **f-h**, Aggregate quantitative data for KW/BW ratio (**f**), CI (**g**) and BUN (**h**). Colors and symbol shapes correspond to genotype, age and treatment groups defined in **e**; *n*, number of mice in each group. Sex information is provided in Supplementary Figure 4. Multiple-group comparisons by one-way ANOVA followed by Tukey's multiple-comparison test, presented as mean ± s.e.m. **i**, Representative hematoxylin and eosin stained histological sections from kidneys with the genotypes, ages and doxycycline/tamoxifen regimens corresponding to the color and symbol shape coding in **e**. At least one histological section from at least one kidney of each mouse in **f-h** was examined. Scale bar, 200 μm. **j**, Time course of change in KW/BW ratio for $Pkd2^{fl/-}$; $Pkd2^{FSF}$; $TetO^{Cre}$; $Rosa^{FlpoER}$ mice treated with doxycycline and tamoxifen (non-cystic, blue) and $Pkd2^{Cre/Flpo}$ mice treated only with doxycycline from P28–42 to inactivate *Pkd2* (cystic, red) or with doxycycline followed by tamoxifen for 7 days beginning at 13 weeks (re-expression, green). Each data point is presented as the mean ± s.e.m.; the Hill slope is +0.22 for the cystic model (red) and −1.70 for the re-expression model (green). Reduction of kidney volume following re-expression of PC2 occurs more rapidly than the increase in volume following inactivation of PC2. Full-length blots are provided as Source Data.

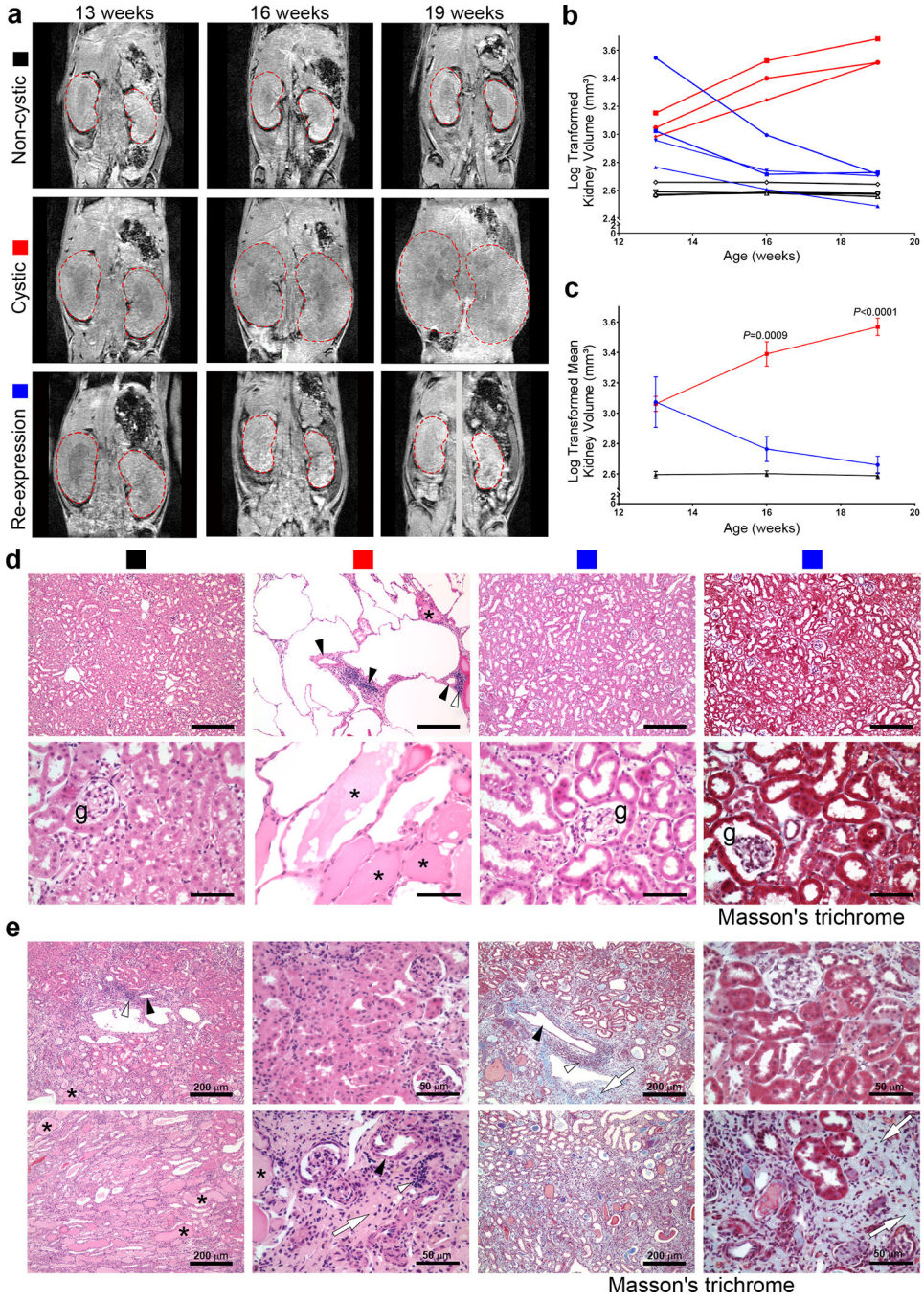

Figure 2 |. Serial imaging shows reduction in total kidney volume following PC2 re-expression.

a, Representative images from MRI studies of individual mice at the indicated ages. All mice had the *Pkd2*$^{Cre/Flpo}$ genotype. “Non-cystic” mice (black square) received neither doxycycline nor tamoxifen; “cystic” mice (red square) received only doxycycline from P28–42; “re-expression” mice (blue square) received doxycycline from P28–42 and tamoxifen for 1 week beginning after the initial MRI at 13 weeks age. Kidneys in the frontal plane are outlined in dashed red lines. The 19-week re-expression mouse (bottom right panel) was rotated during imaging so the frontal plane for each kidney was obtained from

different slices of the same MRI acquisition. **b**, Log transformed kidney total volumes over time plotted for individual mice. **c**, Mean log transformed kidney volumes for each treatment group. Colors in **b** and **c** correspond to treatment groups labeled in **a**. Multiple group comparisons were performed using two-way ANOVA followed by Tukey's multiple comparison test and are presented as the mean ± s.e.m. Representative frontal plane MR images for all mice are provided in Supplementary Figure 6 and absolute kidney volume measurements are provided in Supplementary Table 1. **d**, Representative histological sections from mice at 19 weeks age with treatments denoted by the colored squares. Hematoxylin and eosin stain for each group and Masson's trichrome stain for the re-expression group (rightmost panel). Absence of significant blue staining in the latter indicates absence of fibrosis after re-expression. Asterisks show proteinaceous deposits in cysts; open arrowheads indicate inflammatory infiltrates occurring near blood vessels marked by black arrowheads; g, glomerulus. At least one histological section from each kidney of the 10 mice in **b** was examined with each stain. Scale bars: upper panels, 200 μm; lower panels, 50 μm. **e**, Hematoxylin and eosin (left four panels) and Masson's trichrome (right four panels) from the mouse in the MRI study with the markedly enlarged kidneys at 13 weeks that showed >6-fold reduction in volume at 19 weeks (see text and images in red box in Supplementary Fig. 6). While some areas appear histologically normal, the incomplete functional recovery in this mouse (elevated BUN, Supplementary Table 1) is correlated with areas of fibrosis and disappearance of tubules (white arrows), occasional inflammatory infiltrates (open arrowheads) sometimes associated with nearby blood vessels (black arrowheads) and dilated tubules with proteinaceous casts (asterisks). At least 3 sections from each kidney of this mouse were examined with each stain.

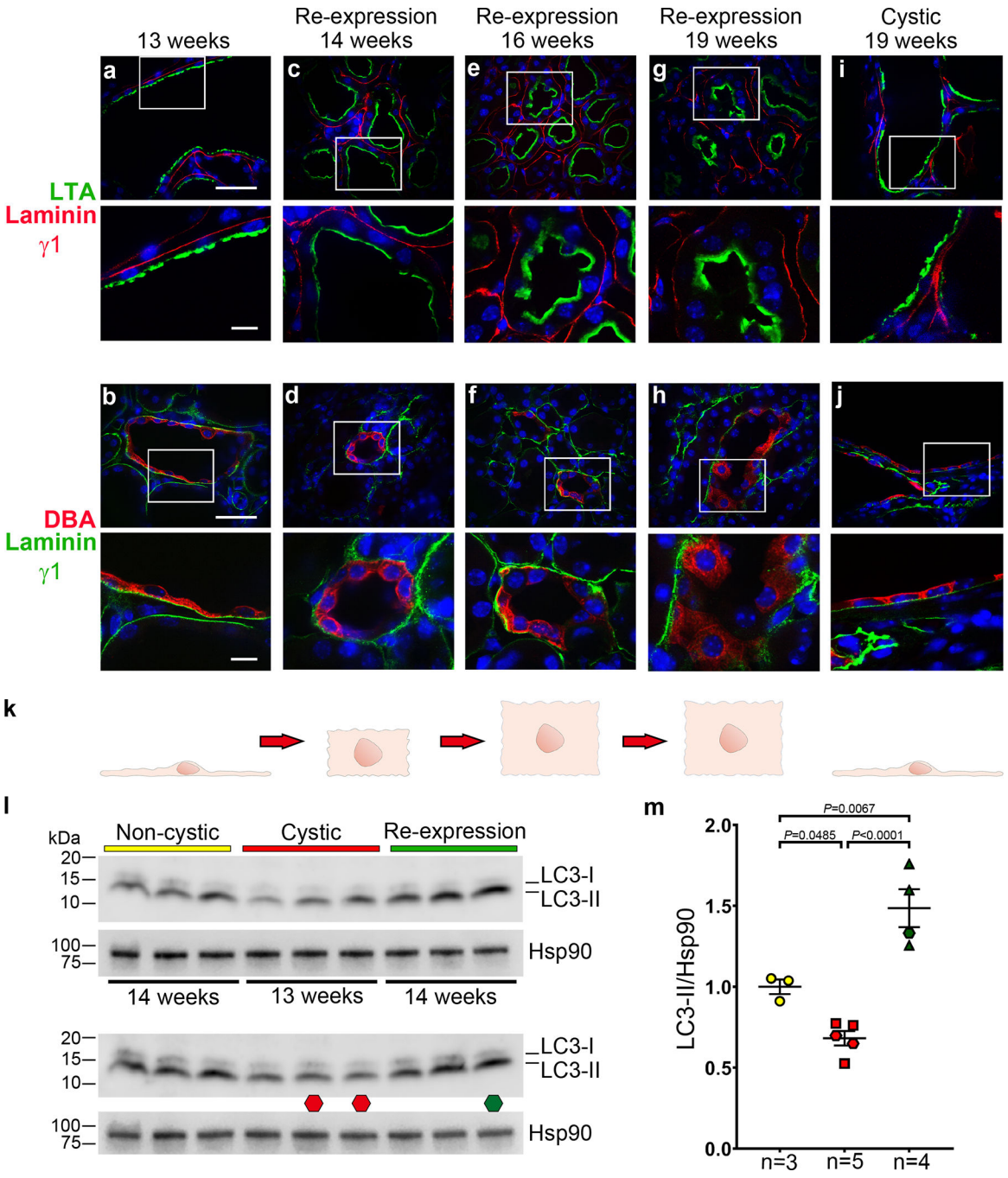

Figure 3 |. Changes of tubule cell shapes following re-expression of PC2.

a-j, Immunohistochemistry of kidneys from doxycycline-treated *Pkd2*$^{Cre/Flpo}$ mice at the indicated ages in the absence (**a, b, i, j,**) or presence (**c-h**) of PC2 re-expression beginning at 13 weeks. Proximal tubules are marked by Lotus tetragonolobus agglutinin (LTA; **a, c, e, g, i**) and collecting ducts are marked by Dolichos biflorus agglutinin (DBA; **b, d, f, h, j**). Tubular basement membranes are marked by laminin γ1 in all images to highlight the relative changes in cell shape from flattened squamoid morphology (**a, b, i, j**) to progressively more cuboidal shape (**c-h**). Nuclei are stained with Hoechst stain (blue). At

least one section from 3 kidneys for each treatment and age group were examined with each nephron segment marker. The lower image in each panel is an enlarged view of the white-boxed regions in the respective upper panel. Scale bars: upper panels, 40 μm; lower panels, 10 μm. **k**, Schematic drawing illustrating the pattern of changes in cell shapes in the corresponding column of images above. **l,m**, Changes in autophagy with *Pkd2* inactivation and re-expression. Immunoblots (**l**) and quantitation of changes in LC3-II expression (**m**). All mice received doxycycline from P28–42 and were fasted for 20 hours and treated with bafilomycin A_1 for 2 hours before harvesting kidney tissue at the indicated ages, which apply to both upper and lower blots. Non-cystic (yellow), no $Pax8^{rtTA}$ allele; cystic (red), $Pkd2^{Cre/Flpo}$ mice; re-expression (green), $Pkd2^{Cre/Flpo}$ mice also treated with tamoxifen at 13 weeks. In **l**, two immunoblots were run to allow comparison of additional samples. The lower immunoblot has the same samples and loading as the upper blot except for two lanes marked by the red octagon at 13 weeks age and one lane marked with the green octagon at 14 weeks which are different biological samples. In **m**, densitometric ratios of LC3-II to Hsp90 for each lane are shown relative to the mean of the ratio in the non-cystic samples, which is set a value of 1.0 to normalize expression in each blot. Hexagons, data from lower blot. Multiple group comparisons were performed using one-way ANOVA followed by Tukey's multiple comparison test and are presented as the mean ± s.e.m. Full-length blots are provided as Source Data.

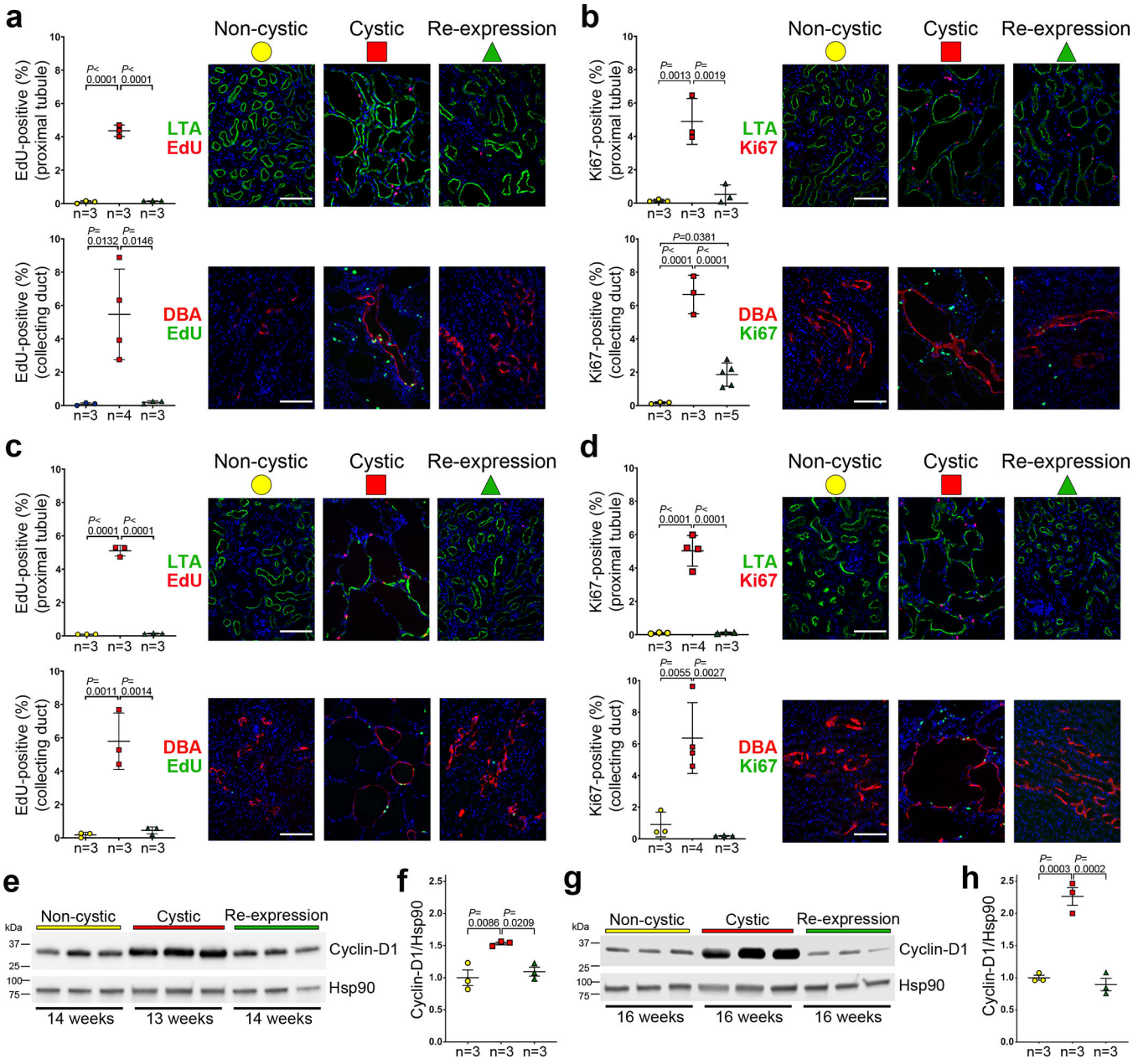

Figure 4 |. Decreased cyst cell proliferation following re-expression of PC2.

a-d, Aggregate quantitative data and representative images showing the percentage of EdU-positive nuclei (**a, c**) and Ki67-positive nuclei (**b, d**) in the kidneys of mice at 14 weeks (**a, b**) and 16 weeks (**c, d**) age. All mice have the *Pkd2*$^{Cre/Flpo}$ genotype. “Non-cystic” mice (yellow circle) received neither doxycycline nor tamoxifen; “Cystic” mice (red square) received only doxycycline from P28–42; “Re-expression” mice (green triangle) received doxycycline from P28–42 and tamoxifen for 1 week beginning at 13 weeks age. The rate of EdU and Ki67 positive nuclei amongst 1,000 nuclei marked by DAPI (blue) in cells positive for Lotus tetragonolobus agglutinin (LTA; proximal tubule) and Dolichos biflorus agglutinin (DBA; collecting duct), respectively, was determined in each mouse. The indicated “*n*” are the number of mice in each group. Scale bars, 100 μm. **e-h**, Changes in cyclin-D1 expression

in kidneys with *Pkd2* inactivation and re-expression. Immunoblots (**e, g**) and quantitation using densitometric ratios (**f, h**) of three biological samples for each treatment indicated by the color key in **a**-**d**. Ages are indicated below the immunoblots. Densitometric ratios of cyclin-D1 to Hsp90 for each lane are shown relative to the mean of the ratio in the non-cystic samples, which is set a value of 1.0. Multiple group comparisons were performed using one-way ANOVA followed by Tukey's multiple comparison test and are presented as the mean ± s.e.m. Full-length blots are provided as Source Data.

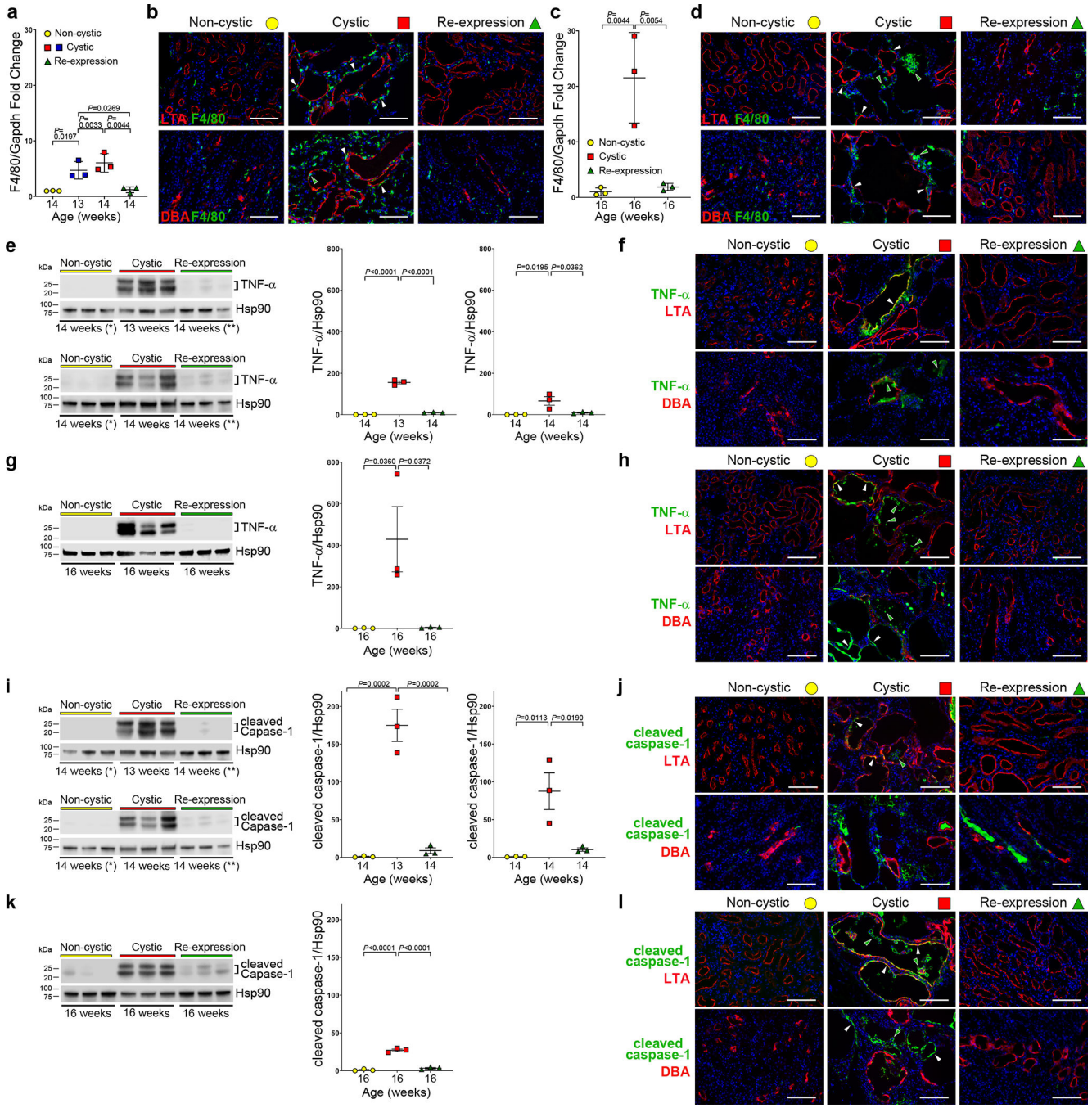

Figure 5 |. Reversal of inflammatory changes in cystic kidneys following PC2-HA re-expression.

a-d, F4/80 mRNA expression in whole kidney lysates (**a, c**) and representative images of F4/80 stained kidney sections (**b, d**) at 14 (**b**) and 16 (**d**) weeks. All mice have the *Pkd2*$^{Cre/Flpo}$ genotype (**a-l**). Color key: non-cystic (yellow), no treatment; cystic (red), doxycycline from P28–42; re-expression (green), doxycycline from P28–42 and tamoxifen for 7 days beginning at 13 weeks. **a,c**, Fold-change mRNA expression at the indicated ages, normalized to Gapdh relative to the mean for non-cystic kidneys which is set to 1.0. **b,d**, F4/80 positive macrophages are increased in cystic kidneys; they appear both

in the pericystic regions (white arrowheads) and on the luminal aspect of cysts (green arrowheads). Macrophages revert to normal expression in kidneys with PC2 re-expression. **e-k**, Changes in TNF-α (**e-h**) and cleaved caspase-1 (**i-l**) expression with *Pkd2* inactivation and re-expression. Shown are immunoblots with quantitation using densitometric ratios (**e, g, i, k**). Samples marked with * and ** (**e, i**) were reloaded on both upper and lower immunoblots to allow comparison to both 13-week (top) and 14-week (bottom) cystic kidneys. Densitometric ratios include both bands for TNF-α (**e, g**) and cleaved caspase-1 (**i, k**) relative to Hsp90; fold-change is shown relative to the mean of the ratio in the non-cystic samples, which is set to 1.0. Multiple group comparisons were performed using one-way ANOVA followed by Tukey's multiple comparison test and are presented as the mean ± SEM. Representative kidney immunocytochemistry images (**f, h, j, l**) from 14 week (**f, j**) and 16 week (**h, l**) kidneys. Cystic kidneys have increased TNF-α (**f, h**) and increased cleaved caspase-1 (**j, l**) expression in a subset of cyst cells (white arrowheads) and cyst lumens (green arrowheads). TNF-α and cleaved caspase-1 immunofluorescence returned to control levels in tissues after re-expression of PC2. LTA, Lotus tetrogonolobus agglutinin (proximal tubule); DBA, Dolichos biflorus agglutinin (collecting duct); nuclei are stained with DAPI (blue). At least one section from 3 kidneys for each treatment and age group were examined for all representative images. Scale bars, 100 μm. Full-length blots are provided as Source Data.

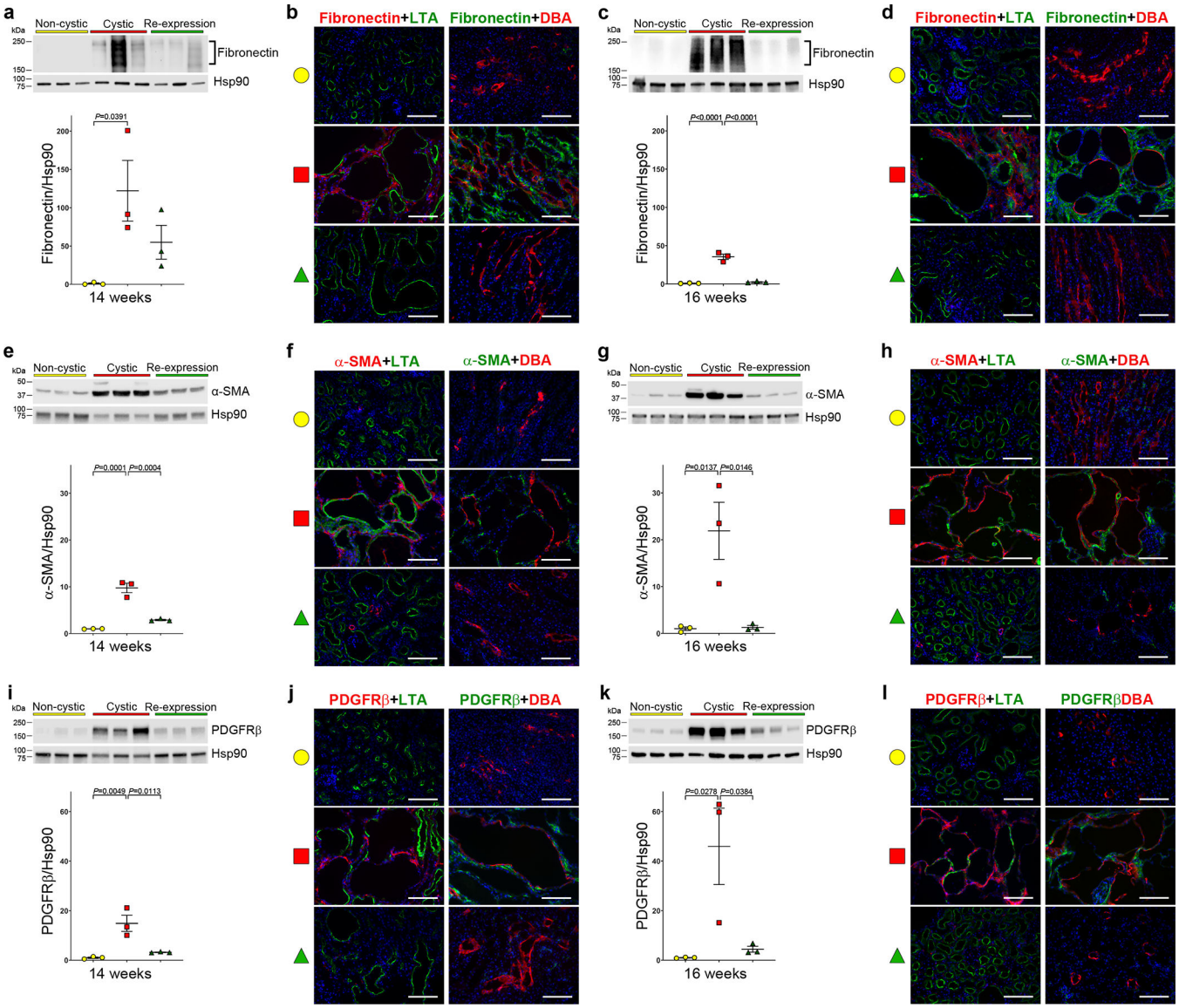

Figure 6 |. Reversal of fibrotic changes in cystic kidneys following PC2-HA re-expression.

a-k, Changes in fibronectin (**a-d**), α-SMA (**e-h**) and PDGFRβ (**i-l**) expression as a function of *Pkd2* inactivation and re-expression. All mice have the *Pkd2*$^{Cre/Flpo}$ genotype. Color key in all panels are: non-cystic (yellow), no treatment; cystic (red), doxycycline from P28–42; re-expression (green), doxycycline from P28–42 and tamoxifen for 7 days beginning at 13 weeks. Shown are immunoblots and quantitation using densitometric ratios at the indicated ages (**a, c, e, g, i, k**). Densitometric ratios relative to Hsp90; fold-change in expression is shown relative to the mean of the ratio in the non-cystic samples on each blot, which is set to a value of 1.0. Multiple group comparisons were performed using one-way ANOVA followed by Tukey's multiple comparison test and are presented as the mean ± s.e.m. Representative kidney immunohistochemistry images (**b, d, f, h, j, l**) from 14-week-old (**b, j, f**) and 16-week-old kidneys (**d, h, l**). Increased fibronectin (**b**, **d**), α-SMA (**f**, **h**) and PDGFRβ (**j**, **l**) expression is present in interstitial areas in cystic kidneys at both time points;

these changes are absent after re-expression of PC2. Each panel in **b**, **d**, **f**, **h**, **j** and **l** is representative of at least one section stained from each of 3 separate kidneys. Scale bars, 100 μm. Full-length blots are provided as Source Data.

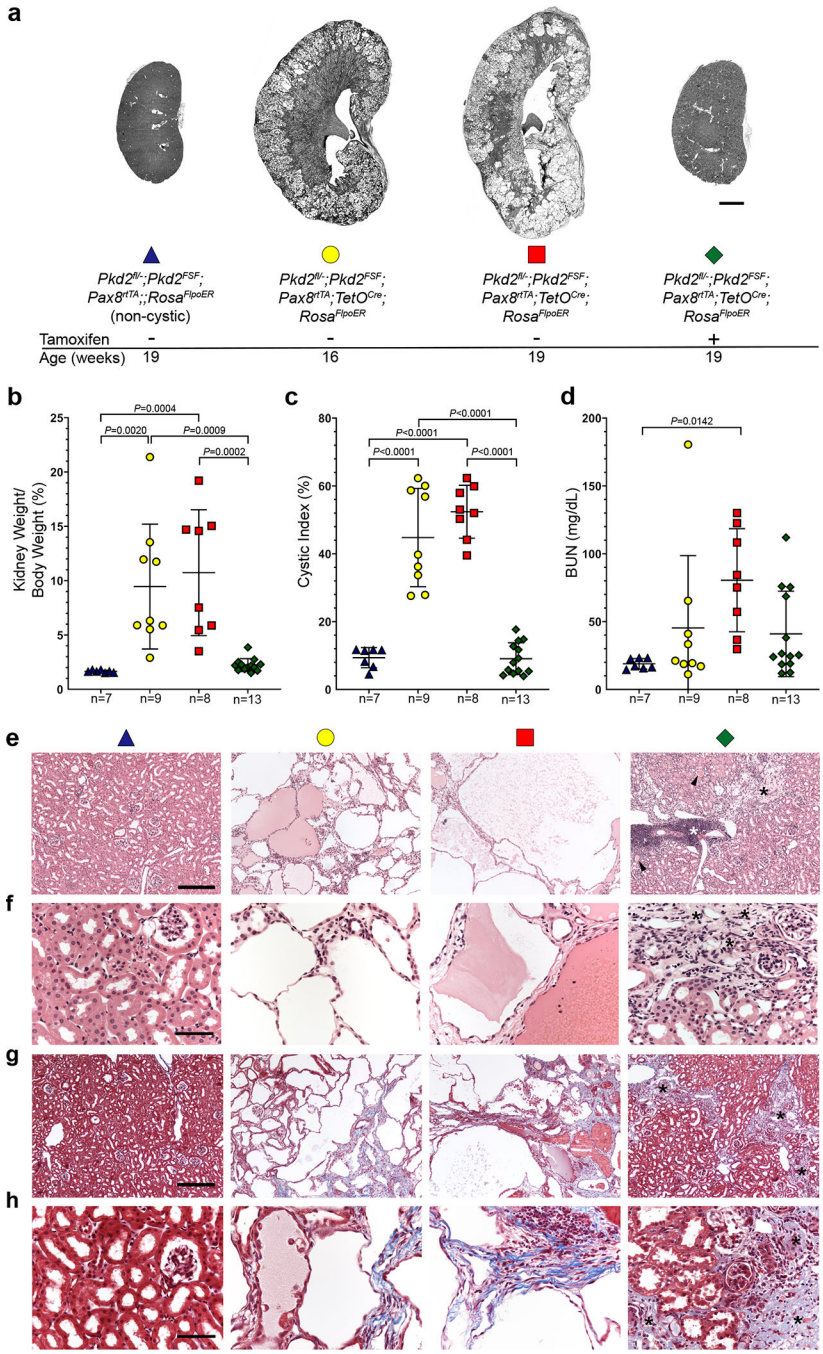

Figure 7 |. Later stage reactivation of *Pkd2* reverses cyst formation but kidney repair is less complete.

a, Representative images of kidneys with the indicated genotypes and ages. All mice received doxycycline (P28–42). Tamoxifen was administered daily for 7 days beginning at 16 weeks age to induce *Pkd2* reactivation in the group indicated with +. Scale bar, 2 mm. **b-d**, Aggregate quantitative data for the indicated parameters; *n*, number of mice in each group. Colors and symbol shapes correspond to genotype and treatment groups indicated in **a**. Sex information is provided in Supplementary Figure 14; *Pkd2* models have

not been reported to have sex dimorphism in disease severity. Multiple-group comparisons by one-way ANOVA followed by Tukey's multiple-comparison test, presented as mean ± SEM. **e**-**h**, Representative hematoxylin and eosin (**e, f**) and Masson's trichrome (**g**, **h**) stained histological sections from kidneys with the genotypes, ages and doxycycline/tamoxifen regimens corresponding to the color coding defined in panel **a**. Kidneys with PC2 re-expression beginning at 16 weeks age (green diamond) show areas of normal morphology with marked resolution of tubule dilation but also have areas of focal inflammation (white asterisks), tubule dilation with protein casts (black arrowheads) and persistence of fibrosis (black asterisks and blue stained areas in **g** and **h**). At least one histological section from at least one kidney of each mouse in **b-d** was examined with both stains. Scale bars: 200 μm (**e, g**); 50 μm (**f, h**).

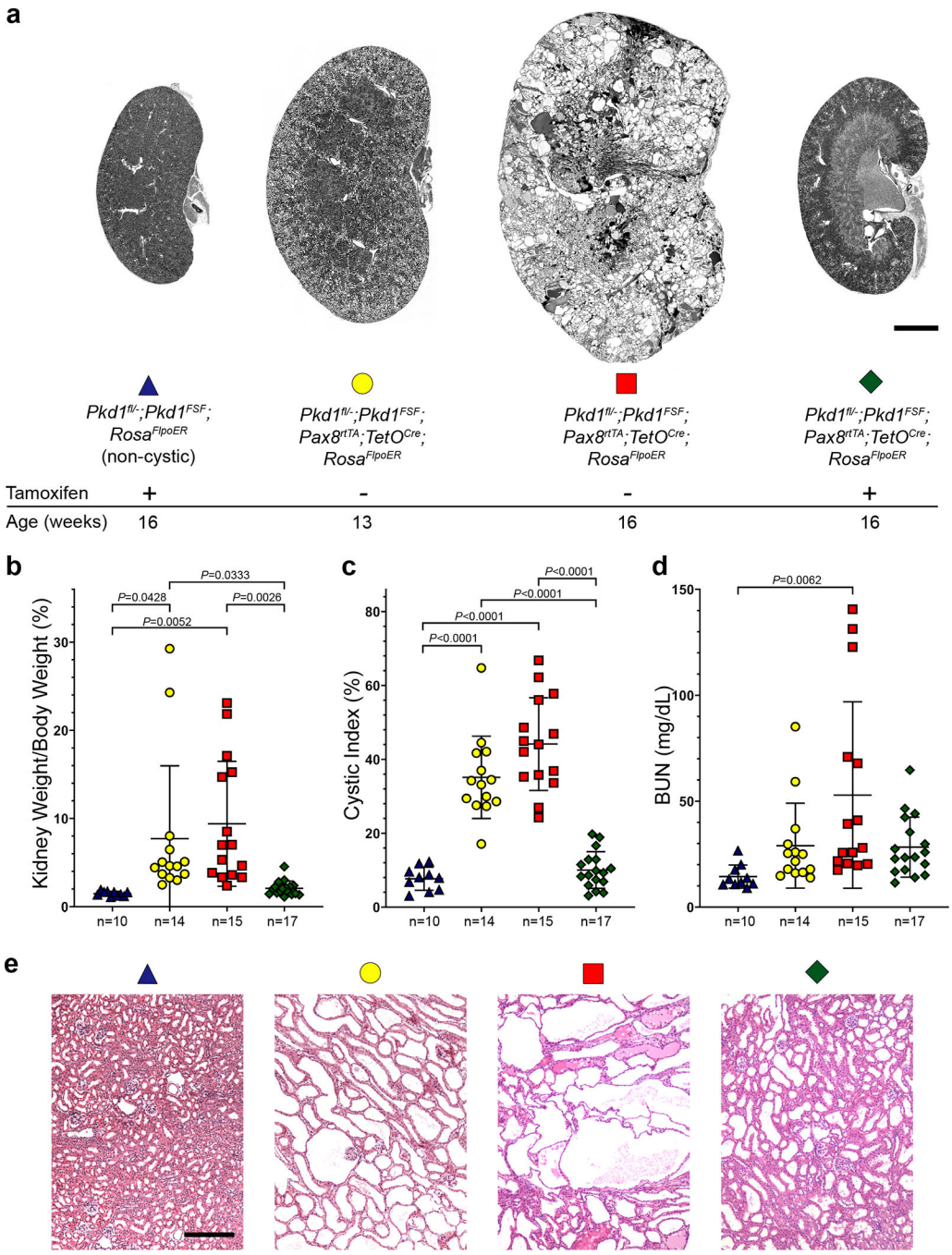

Figure 8 |. Reactivation of *Pkd1* reverses cyst formation.

a, Representative images of kidneys with the indicated genotypes and ages. All mice received doxycycline (P28–42). Tamoxifen was administered daily for 7 days beginning at 13 weeks age to induce *Pkd1* reactivation in the group indicated with +. Scale bar, 2 mm. **b-d**, Aggregate quantitative data for the indicated parameters; *n*, number of mice in each group. Colors and symbol shapes correspond to genotype and treatment groups defined in **a**. Sex information is provided in Supplementary Figure 16. Multiple-group comparisons by one-way ANOVA followed by Tukey's multiple-comparison test, presented as mean ± s.e.m.

e, Representative hematoxylin and eosin stained histological sections from kidneys with the genotypes, ages and doxycycline/tamoxifen regimens corresponding to the color coding defined in panel **a**. Mild persistent tubular dilation is present in areas of the 16-week-old kidneys following re-expression of *Pkd1* (green diamond). At least one histological section from at least one kidney of each mouse in **b-d** was examined. Scale bar, 200 μm.